Published July 25, 2011

D4cpv-calsequestrin: a sensitive ratiometric biosensor accurately targeted to the calcium store of skeletal muscle

Monika Sztretye, Jianxun Yi, Lourdes Figueroa, Jingsong Zhou, Leandro Royer, and Eduardo Ríos

Section of Cellular Signaling, Department of Molecular Biophysics and Physiology, Rush University, Chicago, IL 60612

Current fluorescent monitors of free [Ca^{2+}] in the sarcoplasmic reticulum (SR) of skeletal muscle cells are of limited quantitative value. They provide either a nonratio signal that is difficult to calibrate and is not specific or, in the case of Forster resonant energy transfer (FRET) biosensors, a signal of small dynamic range, which may be degraded further by imperfect targeting and interference from endogenous ligands of calsequestrin. We describe a novel tool that uses the cameleon D4cpv, which has a greater dynamic range and lower susceptibility to endogenous ligands than earlier cameleons. D4cpv was targeted to the SR by fusion with the cDNA of calsequestrin 1 or a variant that binds less Ca^{2+}. "D4cpv-Casq1," expressed in adult mouse at concentrations up to 22 µmole/liter of muscle cell, displayed the accurate targeting of calsequestrin and stayed inside cells after permeabilization of surface and t system membranes, which confirmed its strict targeting. FRET ratio changes of D4cpv-Casq1 were calibrated inside cells, with an effective K_D of 222 µM and a dynamic range $[(R_{max} - R_{min})/R_{min}]$ of 2.5, which are improvements over comparable sensors. Both the maximal ratio, R_{max}, and its resting value were slightly lower in areas of high expression, a variation that was inversely correlated to distance from the sites of protein synthesis. The average $[Ca^{2+}]_{SR}$ in 74 viable cells at rest was 416 µM. The distribution of individual ratio values was Gaussian, but that of the calculated $[Ca^{2+}]_{SR}$ was skewed, with a tail of very large values, up to 6 mM. Model calculations reproduce this skewness as the consequence of quantifiably small variations in biosensor performance. Local variability, a perceived weakness of biosensors, thus becomes quantifiable. It is demonstrably small in D4cpv. D4cpv-Casq1 therefore provides substantial improvements in sensitivity, specificity, and reproducibility over existing monitors of SR free Ca^{2+} concentration.

INTRODUCTION

The processes required for action potential–induced contraction of skeletal muscle cells include the release into the cytosol of >200 µmoles of Ca^{2+} per liter of myoplasm (Pape et al., 1993; Baylor and Hollingworth, 2003). This amounts to between 10 and 20% of the total Ca^{2+} that can be released from the storage organelle (Pape et al., 1993; Pizarro and Ríos, 2004; Launikonis et al., 2006; Rudolf et al., 2006), which for fast-twitch fibers at rest (in a variety of preparations) is estimated at between 1 and 5 mmol per liter of myoplasm (e.g., Schneider et al., 1987; Jong et al., 1993; Fryer and Stephenson, 1996; Owen et al., 1997). In some cells at 37°C, the rise time of the Ca^{2+} transient may be as little as 1 ms. The rise time is approximately equal to the time when Ca^{2+} is being released. Therefore, a flux averaging ~200 mM/s should operate during that time.

For such large flux to peak within 1 ms and then turn off equally rapidly, it is necessary to open and close large numbers of channels in a highly coordinated fashion. In skeletal muscle, the mechanisms for synchronously opening and closing channels include control by the voltage sensor of the transverse-tubular membrane, the dihydropyridine receptor (DHPR), but additionally must have other contributions. The need for extra mechanisms of release activation or termination is evident in the fact that the flux of Ca^{2+} release elicited by voltage clamp pulse depolarization rises to an early peak and then spontaneously and rapidly decays, even though the voltage sensor remains in its fully activating condition, and, as stated above, only a fraction of the sarcoplasmic reticulum (SR) content has been released (e.g., Royer et al., 2008, 2010).

One prominent factor in cardiac myocytes is the terminating effect of depletion, which appears to take place when $[Ca^{2+}]_{SR}$ reaches threshold levels that are locally very well defined, and far removed from full depletion (see Zima et al., 2010) . In skeletal muscle, however, a

Correspondence to Eduardo Ríos: erios@rush.edu

L. Royer's present address is Institut interdisciplinaire de Neurosciences, Université Bordeaux 2, 33077 Bordeaux cédex, France.

Abbreviations used in this paper: BAPTA, 1,2-bis(o-aminophenoxy)ethane-*N*,*N*,*N*′,*N*′-tetraacetic acid; BS, Black Swiss; EYFP, enhanced yellow fluorescent protein; FDB, flexor digitrorum brevis; FRET, Forster resonant energy transfer; SEER, shifted excitation and emission ratioing; SFP, simulated fluorescence process; SR, sarcoplasmic reticulum; SW, Swiss Webster.

The Rockefeller University Press $30.00
J. Gen. Physiol. Vol. 138 No. 2 211–229
www.jgp.org/cgi/doi/10.1085/jgp.201010591

Supplemental Material can be found at:
http://jgp.rupress.org/content/suppl/2011/07/22/jgp.201010591.DC1.html

Published July 25, 2011

similarly clear-cut inhibitory effect of depletion has not been unequivocally demonstrated (for review see Ríos et al., 2006). Evidence for such an effect will be considered in a companion paper (see Sztretye et al. in this issue).

The lack of a reliable technique to actually measure $[Ca^{2+}]_{SR}$ in skeletal muscle has hampered the elucidation of its putative regulatory roles. Until now, the most sensitive measurements have been done with the synthetic nonratiometric dye fluo-5N (Kabbara and Allen, 2001; Ziman et al., 2010), which loads the SR but also the cytosol and other organelles, making quantitative evaluations difficult. In principle, cameleon biosensors (reviewed by Palmer and Tsien, 2006) should not have the same problems, by virtue of their ratiometric cancellation of artifacts and their presumably specific targeting. But the actual results on skeletal SR obtained with the D1ER cameleon have not quite matched its promise. The three published studies (Rudolf et al., 2006; Canato et al., 2010; Jiménez-Moreno et al., 2010) obtained interesting results but found other problems, related to the cameleon's low dynamic range, a high Ca^{2+} affinity that could result in its saturation, and apparent variations in performance in individual cells.

To circumvent the problems mentioned above, we adopted the biosensor approach, with two changes. Instead of the cameleon D1 we used D4, the product of a computational redesign aimed at removing interference by calmodulin (Palmer et al., 2006). D4 has the additional advantage of a substantially greater dynamic range when the acceptor fluorophore is circularly permuted Venus (hence D4cpv).

Additionally, and given the less than ideal features in the expression and targeting of D1ER (which will be demonstrated below), we chose a radically different strategy for SR targeting. SR targeting is accomplished in D1ER by placing the signal sequence of calreticulin at the N terminus and the KDEL ER retention and retrieval signal at the C terminus (Miyawaki et al., 1997). Our approach consists instead of fusing D4cpv with calsequestrin. This was done under the expectation that the fusion protein would retain the extraordinarily precise targeting of calsequestrin, which is restricted not just to the SR lumen, but within the SR resides in the terminal cisternae. Mindful of the fact that calsequestrin is the most important Ca^{2+}-binding protein of the SR, we repeated the measurements using a mutant of reduced binding ability. Additionally, we checked whether the monitor modified in any way the variable that it measures (Sztretye et al., 2011).

In this paper we describe the technique, evaluate targeting of the biosensor and compare it with that of D1ER, provide measures of expression density, and calibrate the biosensor in situ. We then use the technique for a determination of resting $[Ca^{2+}]_{SR}$.

In an accompanying paper we use the biosensor to measure $[Ca^{2+}]_{SR}$ dynamically, together with Ca^{2+} release flux on the same cells (Sztretye et al., 2011). These measurements, which to our knowledge are the first in the literature, were combined to derive Ca^{2+} release permeability and its changes when prolonged pulses cause depletion. Unexpected properties found for permeability in the wild type prompted us to then repeat the combined measurements in mice engineered for complete lack of calsequestrin 1 (Sztretye et al., 2011).

MATERIALS AND METHODS

Assembly of the biosensors

Here we use the term "Casq" to name the protein calsequestrin, its coding DNA, and its gene. Two D4cpv fusion plasmids were assembled: D4cpv-Casq1 and D4cpv-δAsp. D4cpv-X is used to designate either or both. Assembly of the D4cpv-X started from pEYFP-N1-dogCasq2 (Terentyev et al., 2003), provided by D. Terentyev (Ohio State University, Columbus, OH) and S. Gyorke (Ohio State University, Columbus, OH), which has the cytomegalovirus promoter, the Casq2 gene, and the code of enhanced yellow fluorescent protein (EYFP) added after a linking segment. The cDNA of mouse Casq1 (Shin et al., 2000), provided by D.-H. Kim (Kwangju Institute of Science and Technology, Buk-gu, Gwangju, Korea), was amplified by PCR with oligonucleotide primers containing the restriction sites of NheI and BglII. pEYFP-N1-dogCasq2 was then digested with the same enzymes to remove the Casq2 coding region. Ligation to the Casq1 PCR product resulted in the plasmid pEYFP-N1-mouseCasq1. D4cpv was cut out from pBAD/D4cpv (a gift from R.Y. Tsien, University of California, San Diego, La Jolla, CA; and A.E. Palmer, University of Colorado at Boulder, Boulder, CO), using restriction sites of BamHI and EcoRI, and inserted at the 3′ end of the linking segment of pEYFP-N1-mouseCasq1, proximal to EYFP. In the final product, the sequence of the linking segment is RSPRPRDNNRRRMDP. A stop codon was introduced at the 3′ end of D4cpv, preventing the expression of EYFP. The same procedure was used with mouse Casq1-δAsp, a deletion variant lacking the last 17 Asp codons (also a gift from D.-H. Kim) to generate D4cpv-δAsp. The N-to-C terminal sequence in the final product is therefore Casq or its variant, linker, and cameleon.

The D1ER gene, inserted in pcDNA3 between HindIII and EcoRI was a gift of R.Y. Tsien.

Biosensor protein synthesis and purification

pBAD/D4cpv (Palmer et al., 2006) was transformed into TOP10 cells (Invitrogen). A single colony was grown overnight at 25°C. The culture was induced by 0.2% arabinose for 8 h. Total protein was extracted with bacterial protein extraction reagent (BPER; Thermo Fisher Scientific) in the presence of protease inhibition cocktail (Sigma-Aldrich). The His-tagged protein was purified using a Ni-NTA agarose column (QIAGEN). The final protein was buffer-exchanged into 10 mM MOPS and 100 mM NaCl, pH 7.4, using a dialysis cassette (Thermo Fisher Scientific).

Transfection of flexor digitrorum brevis (FDB) muscles in adult mice and isolation of single cells

Protocols were approved by the Institutional Animal Care and Use Committee of Rush University, which found them consistent with their ethical standards. The present results were collected from 170 7–12-wk-old mice (*Mus musculus*; Black Swiss [BS; before 7 January 2010] or Swiss Webster [SW], afterward). The method of transfection is adapted from DiFranco et al. (2006). The ventral side of both hind paws of 2-mo-old mice anaesthetized by isoflurane was cleaned with 75% ethanol. 10 µl of 2 mg/ml

Published July 25, 2011

hyaluronidase in saline was injected into the center of each paw through a 29-gauge needle. 1 h later, 15 µl of plasmid solution (20 µg DNA in sterile saline) was injected subcutaneously. 10 min later, two sterilized gold plated stainless steel acupuncture needles were placed subcutaneously at the starting lines of paw and toes, separated ∼9 mm. 20 pulses of 100 V/cm and 20 ms were applied at 1 Hz (ECM 830 Electro Square Porator; BTX). 4–7 d later, the animal was sacrificed by CO_2 inhalation, and FDB muscles were removed for imaging or functional studies. The methods of cell separation, voltage clamping, recording with a cytosolic Ca^{2+} indicator and analysis were as described by Royer et al. (2008), where additional details can be found. Experiments were performed at 20–22°C in "external" solution.

Solutions

"External": 140 mM TEA-CH_3SO_3, 1 mM $CaCl_2$, 3.5 mM $MgCl_2$, 10 mM Hepes, 1 mM 4-AP, 0.5 mM $CdCl_2$, 0.3 mM $LaCl_3$, 0.001 mM TTX (citrate), and 0.05 mM BTS (*N*-benzyl-p-toluene sulphonamide; Sigma-Aldrich). pH was adjusted to 7.2 with TEA-OH and osmolality was adjusted to 320 mOsm with TEA methanesulfonate.

Internal solutions (in pipette) were either EGTA or 1,2-bis (o-aminophenoxy)ethane-*N*,*N*,*N*′,*N*′-tetraacetic acid (BAPTA). EGTA: 110 mM *N*-methylglucamine, 110 mM L-glutamic acid, 10 mM EGTA, 10 mM Tris, 10 mM glucose, 5 mM Na ATP, 5 mM phosphocreatine Tris, 0.1 mM rhod-2, 3.56 mM $CaCl_2$, and 7.4 mM $MgCl_2$ were added for a nominal 1 mM [Mg^{2+}] and 100 nM [Ca^{2+}]. BAPTA: 110 mM *N*-methylglucamine, 110 mM L-glutamic acid, 5 mM BAPTA, 10 mM Tris, 10 mM glucose, 5 mM Na ATP, 5 mM PC Tris, 0.1 mM rhod-2 or 0.075 mM X-rhod-1, 1.81 mM $CaCl_2$, and 6.96 mM $MgCl_2$ for a nominal 1 mM [Mg^{2+}] and 100 nM [Ca^{2+}]. pH was set to 7.2 with NaOH and osmolality to 320 mOsm with *N*-methylglucamine. The amounts of added Ca^{2+} and Mg^{2+} were calculated using Ca^{2+} dissociation constants of 428 nM for EGTA (Royer et al., 2008) and 200 nM for BAPTA (Wu et al., 1996); the near equality of their free [Ca^{2+}] after at least 30 min of establishing whole-cell patch was verified with ratiometric measurements using indo-1.

"Relaxing" solution was used both for application and washout of saponin. It contained 150 mM K glutamate, 10 mM Hepes, 2 mM $MgCl_2$, and 1 mM EGTA. pH was adjusted to 7.2 with KOH and osmolality to 320 mOsm with potassium glutamate.

"Depleting cocktail": 1 mM 4-chloro-M-cresol (4-CMC), 10 mM caffeine, 0.05 mM cyclopiazonic acid (CPA), 0.05 mM 2.5-di(tert-butyl)-1,4-hydroquinone (TBQ), 0.05 thapsigargin (TG), and 0.05 BTS.

Voltage clamp

The whole-cell patch clamp technique follows the implementation of Wang et al. (1999), with changes described by Royer et al. (2008). The clamped cells were stable in BAPTA, as ascertained by the stability of series resistance, linear capacitance (C_m), which averaged 1.8 nF in 119 cells, charging time constant, and holding current, which ranged from 1 to 10 nA in different cells. The Ca^{2+} transients elicited by depolarization were fast, graded with membrane voltage V_m, and homogeneous, which is consistent with good membrane voltage control. The actual recording of Ca^{2+} transients was started in most cases after ∼35 min of stable holding at −80 mV, a time when the concentration of EGTA or BAPTA inside the cell was at a substantial fraction of the solution values, which along with the presence of BTS caused complete abolition of contractile responses. Command potentials were blunted with 0.6-ms duration ramps to avoid saturation of the headstage. Nonlinear capacitive ("charge movement") currents $I_Q(t)$ obtained by conventional subtraction of scaled controls and baseline correction were integrated to calculate intramembranous charge transfers Q_m (Q_{ON} and Q_{OFF}) as functions of V_m. The functional dependence was fitted with the "Boltzmann" function: $Q_{max}/\{1 + \exp[-(V_m - V_T)/K]\}$ to derive the amount of mobile charge Q_{max}, transition voltage V_T, and limiting logarithmic slope $1/K$. The average values of these parameters were not statistically significantly different than in our previous works with this technique (Royer et al., 2008, 2010). Electrophysiological properties (C_m, holding current, and charge movement parameters) were evaluated in all cells and found to be within limits of normality in every cell included in the measurement of resting $[Ca^{2+}]_{SR}$ reported below.

Cytosolic Ca^{2+} measurements

Ca^{2+} transients and release flux are examined in parallel with $[Ca^{2+}]_{SR}$ in the companion paper (Sztretye et al., 2011), which describes the relevant methods. For the present paper, every cell that was studied under voltage clamp also had the high affinity, long wavelength Ca^{2+} monitor X-rhod-1 introduced via the pipette. This was done both to use cytosolic Ca^{2+} transients for evaluation of the cell's functional state and in order not to introduce an additional variable by having cytosolic dye in some but not all experiments.

Membrane permeabilization

Both for calibration purposes and a test of retention of the biosensors inside organelles, some cells were membrane permeabilized. This was done by exposure of cells inside the experimental chamber, for 4 min, to 0.005% saponin in either EGTA or relaxing solution.

Confocal imaging of biosensor fluorescence and determination of free [Ca^{2+}]

Fluorescence of the biosensors, either purified or expressed within cells, was imaged on a confocal microscope (SP2 acousto-optical beam splitter [AOBS]; Leica) under excitation at 458 nm. For initial exploration of the location of the expressed biosensors, the collection technique optimized spatial resolution. Thus, for increased input of emitted light, fluorescence was collected in a single range, extending between 470 and 560, and at a long integration time at each pixel (5 ms per 512 pixel line), setting the confocal pinhole at 1 Airy disk radius. The noise was reduced further by image averaging, and the resolution was improved further by acquiring z stacks, which could be later processed for deblurring. For determination of [Ca^{2+}], we collected "Forster resonant energy transfer (FRET) pairs;" namely, light of intensity F_1, also referred to as F_{donor}, emitted between 470 and 510 nm, and F_2 or $F_{acceptor}$, between 520 and 580 nm, at 0.24 µm pixel interval, at a frequency of 800 Hz (one line every 1.25 ms), with the pinhole radius set at its maximum. These settings resulted in greater speed of acquisition (important to resolve rapid changes in $[Ca^{2+}]_{SR}$) but much lower spatial resolution.

Imaging was either 2-D ($F_j(x,y)$; example raw images are shown in Fig. S1) or line scan ($F_j(x,t)$; see Fig. 2). 3-D reconstructions (examples in Fig. 1) were derived from z stacks $F_i(x,y,z)$ of single or dual "channels" (i.e., spectral acquisition ranges). Images could be analyzed directly, pixel by pixel, or after spatial averaging, to derive biosensor concentration or Ca^{2+} concentration. As examples, Fig. 2 (C and D) shows line scans $F_j(x,t)$. The graph in Fig. 2 E plots their spatial averages F_j, and the black line shows the derived concentration of biosensor (calculated using Eq. A6 in the Appendix).

The "FRET ratio" R was calculated as $(F_2 - \text{Background}_2)/(F_1 - \text{Background}_1)$ without correction for non-FRET components in F_2. F_j could be a pixel value or an average. $[Ca^{2+}]_{SR}$ was calculated from the ratio as

$$[Ca^{2+}] = \left\{(\beta K_D)^n \frac{R - R_{min}}{R_{max} - R}\right\}^{1/n} \quad (1)$$

where $\beta = F_1$ Ca^{2+}-free/F_1 Ca^{2+}-saturated. Values of R_{min}, R_{max}, and βK_d are derived from calibration experiments described in Results

Published July 25, 2011

(Figs. 5–7). For reasons detailed with Fig. 6, the stoichiometry factor n was set to 1.

Simulations presented in Discussion start from an assumed distribution of $[Ca^{2+}]_{SR}$, from which a value of R is calculated by solving Eq. 1:

$$R = \frac{R_{min}(\beta K_D)^n + R_{max}[Ca^{2+}]^n}{(\beta K_D)^n + [Ca^{2+}]^n} \quad (2)$$

Co-staining and immunofluorescence

In selected cases, cells expressing biosensors were costained with di-8-ANEPPS, a marker of surface and t tubule membranes, or MitoTracker Deep Red. Both stains were obtained from Invitrogen. Cells were exposed to either external solution with 5 µM di-8-ANEPPs for 20 min then thoroughly washed in external solution, or 5 µM MitoTracker for 15 min, then washed. Di-8-ANEPPs was excited at 458 nm, and the emitted light was collected between 600 and 750 nm. MitoTracker Deep Red was excited at 633 nm, and the emitted light collected was between 650 and 750 nm. In costaining experiments, the range of biosensor emission was 470 to 542 nm, to ensure minimal interference from the long wavelength stain. The interference in that range by fluorescence from the long wavelength stains was measured in cells without the biosensor. Autofluorescence was evaluated without either biosensor or costains in the same ranges of emission. For Di-8-ANEPPS, it was <20% of the lowest values detected in cells expressing the biosensors but at least 10 times greater than the autofluorescence excited by radiation of 458 nm in the same range. For MitoTracker Deep Red, the measured fluorescence was not visually different from background. Given these observations, no corrections were made for interference in costaining experiments.

Deblurring and 3-D rendering

"z stacks" of a variable number of xy scans (26–49) were acquired at 0.05–0.1-µm pixel distance and 0.12–0.15-µm vertical intervals and deblurred by constrained iterative deconvolution that used all images in the stack (Agard et al., 1989; van der Voort and Strasters, 1995) with a point spread function (PSF) determined in our microscope (full width at half maximum in the xy plane was 0.45 µm, and in the z direction it was 1.15 µm). The deblurred set was represented or "rendered" in 3-D using the "Simulated Fluorescence Process" (SFP) algorithm (Messerli et al., 1993.)

Immunocytochemistry

Single fibers were dissociated from FDB muscles and transferred to collagen-coated glass-bottom Petri dishes. The fibers were allowed to attach for 10 min at room temperature and then fixed with 4% paraformaldehyde in 100 mM phosphate buffer, pH 7.4. After fixation, the fibers were incubated for 15 min with 100 mM glycine in PBS, pH 7.4, to quench the residual paraformaldehyde. The fibers were then permeabilized in 0.5% Triton X-100 for 15 min at room temperature. Nonspecific binding sites were blocked by incubation with 10% normal goat serum in PBS overnight at 4°C. The fibers were then incubated with anti-Casq1 antibody (1:1,000, MA3-919; Thermo Fisher Scientific) for 2 h at room temperature. After washes with PBS, the fibers were incubated with Cy5-conjugated goat anti–mouse antibody (1:200; Jackson ImmunoResearch Laboratories, Inc.) for 1 h at room temperature. 3-D stacks of confocal images were acquired with a laser scanning microscope (SP2 AOBS; Leica).

Online supplemental material

Fig. S1 shows an example of 3-D image reconstruction in a dually stained cell with low biosensor expression, which allows for better visualization of the relationship between SR-targeted biosensor and t tubule stain. Figs. S2–4 illustrate spatial aspects of the expression of D1ER. Fig. S5 illustrates change in FRET ratio of D1ER in a cell exposed to a depletion cocktail. The supplemental text section describes structural and functional aspects of the expression of D1ER. Online supplemental material is available at http://www.jgp.org/cgi/content/full/jgp.201010591/DC1.

RESULTS

D4cpv-Casq1 expresses selectively inside terminal cisternae of the SR

50–70% of the cells separated enzymatically from FDB muscles of transfected mice were found to express two fusion variants of D4cpv, namely D4cpv-Casq1 and D4cpv-δAsp (collectively named D4cpv-X). The topography of expression is illustrated in Fig. 1 A for a cell expressing D4cpv-δAsp. In raw xy images, the fluorescence was found in bands, at sarcomeric spacing (∼2.0 µm in these cells). Fig. 1 A is a 3-D reconstruction (or rendering) of a vertical stack of xy images, after deblurring (individual members of the raw stack are in Fig. S1). The rendering reveals within every band a double row of high expression density. The structure is similar to that found after the same image refinement in nontransfected FDB cells immunostained for calsequestrin 1 (Fig. 1 B), although an additional, faint area of biosensor expression is seen at the center of every double row (Fig. 1 A), and again as a small "bump" in alternating nadirs of the distribution profile plotted in Fig. 1 H. The similarity between the placement of biosensor and native calsequestrin indicates that the biosensor is targeted to terminal cisternae by the fused calsequestrin.

Additional evidence of targeting was found in cells expressing D4cpv-X that were stained by brief exposure to di-8-ANEPPS, which marks plasma membrane and t tubules upon brief exposure. An example is in Fig. 1. z stacks of fluorescence of biosensor and di-8-ANEPPS were acquired simultaneously and deblurred. Fig. 1 (C and D) shows corresponding individual frames of each stack after deblurring. Fig. 1 (E and F) shows separate 3-D renderings of the deblurred stacks. The qualitative features of Fig. 1 E are similar to those of the stack illustrated in Fig. 1 A.

In Fig. 1 G is a joint 3-D rendering of both stains. Note that the t tubular stain (in green) is visible on the cell surface, whereas in the cell interior it appears only in sparse pixel-size spots. The image in Fig. 1 G is not a standard overlay, but a display of both stacks by the SFP (Messerli et al., 1993). This algorithm is designed for a realistic view, with visual cues of volume and relative positioning, which in the present example reflect the fact that the biosensor, in red, surrounds the t tubules like a sheath, in agreement with the relative location of terminal cisternae and t tubules. An analogue rendering in a case where the expression of biosensor was more sparse (presented in Fig. S1) reveals more clearly the t tubules

Published July 25, 2011

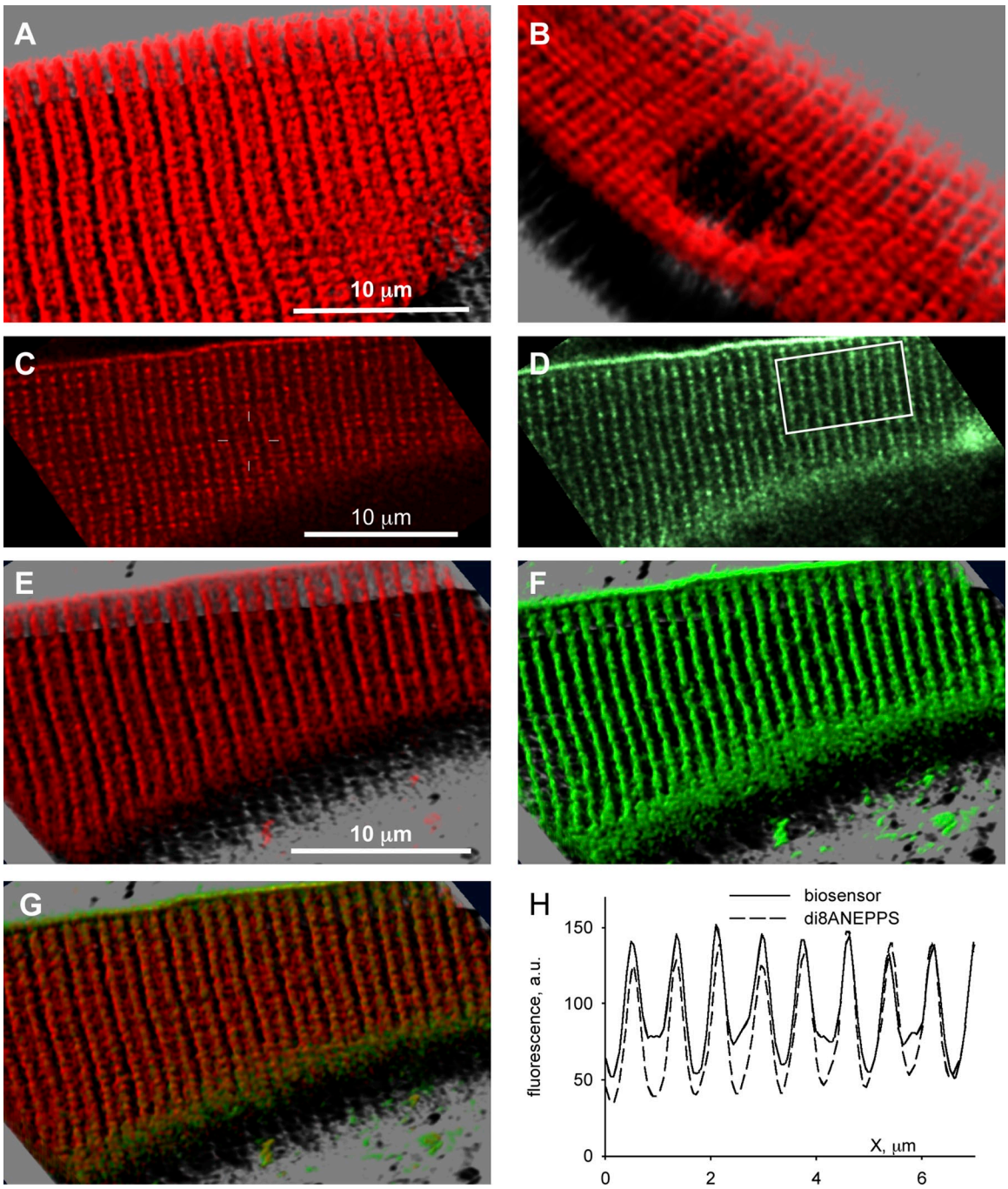

Figure 1. Location of the expressed biosensor. (A and B) 3-D renderings of z stacks of confocal images, deblurred by all-neighbors deconvolution and then displayed by the SFP algorithm (details given in Materials and methods). (A) A cell expressing D4cpv-δAsp; the stack comprises 30 images at 0.12-μm intervals. (B) A wild-type cell fixed and immunostained using Cy5-conjugated anti-calsequestrin antibody. The stack comprises 26 images, at 0.15-μm intervals. ID: 020411a series 89, 051007b series 51. (C–H) Images from two z stacks (of 40 "slices" each, at 0.12-μm intervals) of a cell expressing D4cpv-δAsp, costained with di-8-ANEPPS. Images were obtained simultaneously for the two stacks. Stacks were deblurred by all-neighbors deconvolution. (C and D) Individual slices at position 24. (C) Biosensor. (D) di-8-ANEPPS. (E and F) Separate 3D renderings. Note the similarity between renderings of biosensor fluorescence in E (costained) and A (biosensor only). (G) Joint 3D rendering of both stacks. di-8-ANEPPS is visible in the cell surface but not in the t tubule network (an observation discussed in text). (H) Profiles $F(x)$, obtained by averaging fluorescence in images C and D over the spatial coordinate transversal to the fiber axis within the boxed region in D. Note the colocalization of both markers. ID: 020411a series 120, slices 24.

within the columns of biosensor. The relative location of sensor and tubules is clearly demonstrated (Fig. 1 H) in plots of fluorescence averaged perpendicularly to the fiber axis within the box marked in Fig. 1 D. Further evidence that the structure containing the biosensor surrounds the tubules, which is consistent with their

Published July 25, 2011

identification with terminal cisternae, is presented in the supplemental materials section.

The present targeting strategy, which consists of fusion of the biosensor with calsequestrin, is different than that driving the biosensor used in previous work, D1ER. To decide whether the alternative strategy altered the cellular location of the biosensor, we obtained similar images in cells from mice transfected with D1ER using identical protocols. As demonstrated in the supplement materials (Figs. S2–S4), the pattern of expression of D1ER was clearly different from that of D4cpv-X. Moreover, we found two patterns in the expression of D1ER, with clearly different features at both the cell and the subsarcomeric level. The supplemental material presents initial attempts to put the regions of high D1ER expression in correspondence with structures of the sarcomere.

The concentration of biosensor can be accurately determined

To quantify the probable perturbation of Ca^{2+} handling that the addition of extrinsic calsequestrin present in the biosensor might induce, we determined the biosensor concentration, S_T. This was done in every cell, based on a metric first introduced by Launikonis et al. (2005) for determining the concentration of Mag-Indo inside organelles.

An adaptation of this metric to its use with FRET biosensors is presented in the Appendix. According to Eq. A6, S_T is proportional to a linear combination of fluorescence intensities F_1 ("donor") and F_2 ("acceptor"). This linear combination was named the "invariant" (Launikonis et al., 2005) to stress its insensitivity to changes in $[Ca^{2+}]$. Fig. 2 demonstrates the defining property of the invariant using dynamic signals from the biosensor upon Ca^{2+} release in a voltage clamped cell. xy images F_1 and F_2 of the cell are shown in Fig. 2 (A and B). Shown in Fig. 2 (C and D) are line scans parallel to the axis of the cell, obtained with large pinhole and low laser intensity (to minimize bleaching). The cell was depolarized as shown from a holding potential of −80 mV. Represented in Fig. 2 E are line averages of the background-corrected fluorescence intensities. The black line in Fig. 2 E is S_T, calculated from the invariant by Eq. A6. It remains steady in spite of large intensity swings in the fluorescence. Fig. 2 F shows the result of combining images A and B according to the invariant formula (Eq. A6). Although the concentration of biosensor reported in the double bands is on average 8 µM, in-between the bands it is close to zero (put simply, both F_1 and F_2 are reduced close to background level). This topography of the calculated concentration is consistent with the localization demonstrated in the earlier figures. In our experience with sensors and dyes, including D1ER, other cameleons directed to mitochondria, as well as "hybrids" of small synthetic dyes and genetically encoded fusion proteins (Bannwarth et al., 2009), only the fusions with calsequestrin variants achieved such a level of topographic specificity.

Using this method, the concentration of D4cpv-X was averaged over a segment of the image comprising the whole width of the cell and 118 µm of its length. Histograms of segment-averaged concentrations are represented in Fig. 3 and summaries are presented in Table I. The histograms show that biosensor concentration varied widely. As demonstrated in Fig. 4 and elsewhere, individual cells could present steep gradients between perinuclear areas of active protein synthesis and areas away from nuclei, or feature long segments with relatively homogeneous concentrations of the protein. The heterogeneity of expression is used later to test for artifacts that could be attributed to the foreign protein.

Fig. 3 illustrates the relative efficiency of expression of the two biosensor variants used, as well as a dependence on two mouse strains. In white is the histogram of concentrations of D4cpv-Casq1, expressed in BS mice. The histograms in gray and black compare expression of D4cpv-Casq1 and D4cpv-δAsp. This was done in SW mice, as the BS strain became unavailable after 7 January 2010. Although no other aspects of the procedure were changed, there was a highly significant difference in the concentration of either expressed protein (1.2–1.5 µmole protein per liter of fiber) with respect to the concentration of D4cpv-Casq1 observed in BS mice (close to 3 µM). Although large for a biosensor, these concentrations will be shown to be trivial relative to the intrinsic concentration of calsequestrin.

Expression of the two biosensor variants could be compared in the SW mice (Table I); D4cpv-δAsp expressed somewhat better, although at levels still far from those observed for D4cpv-Casq1 in the BS strain.

Permeabilization of plasma membrane did not cause loss of biosensor

The accuracy of biosensor targeting was tested by membrane permeabilization. Fig. 4 A shows the distribution of D4cpv-Casq1 in a cell with intact plasmalemma. In Fig. 4 B is the same cell, first exposed to a saponin-containing solution for 4 min, then immersed in a solution with 100 nM $[Ca^{2+}]$ and measured 6 min later. The concentration of biosensor, calculated per unit of fiber volume, had decreased slightly (from an average of 3.11 µM in Fig. 4 A to 2.90 µM in Fig. 4 B). This decrease, however, was probably caused by the increase in cell volume. The total content, calculated by integrating the concentration in the volume, went from 2.29 arbitrary units (au) in Fig. 4 A to 2.44 au in Fig. 4 B, an increase of 6%. On average, the biosensor content decreased, but not significantly so (average change: −7% of the initial value; SEM 8%; 14 cells, 10 with D4cpv-Casq1 and 4 with D4cpv-δAsp).

Published July 25, 2011

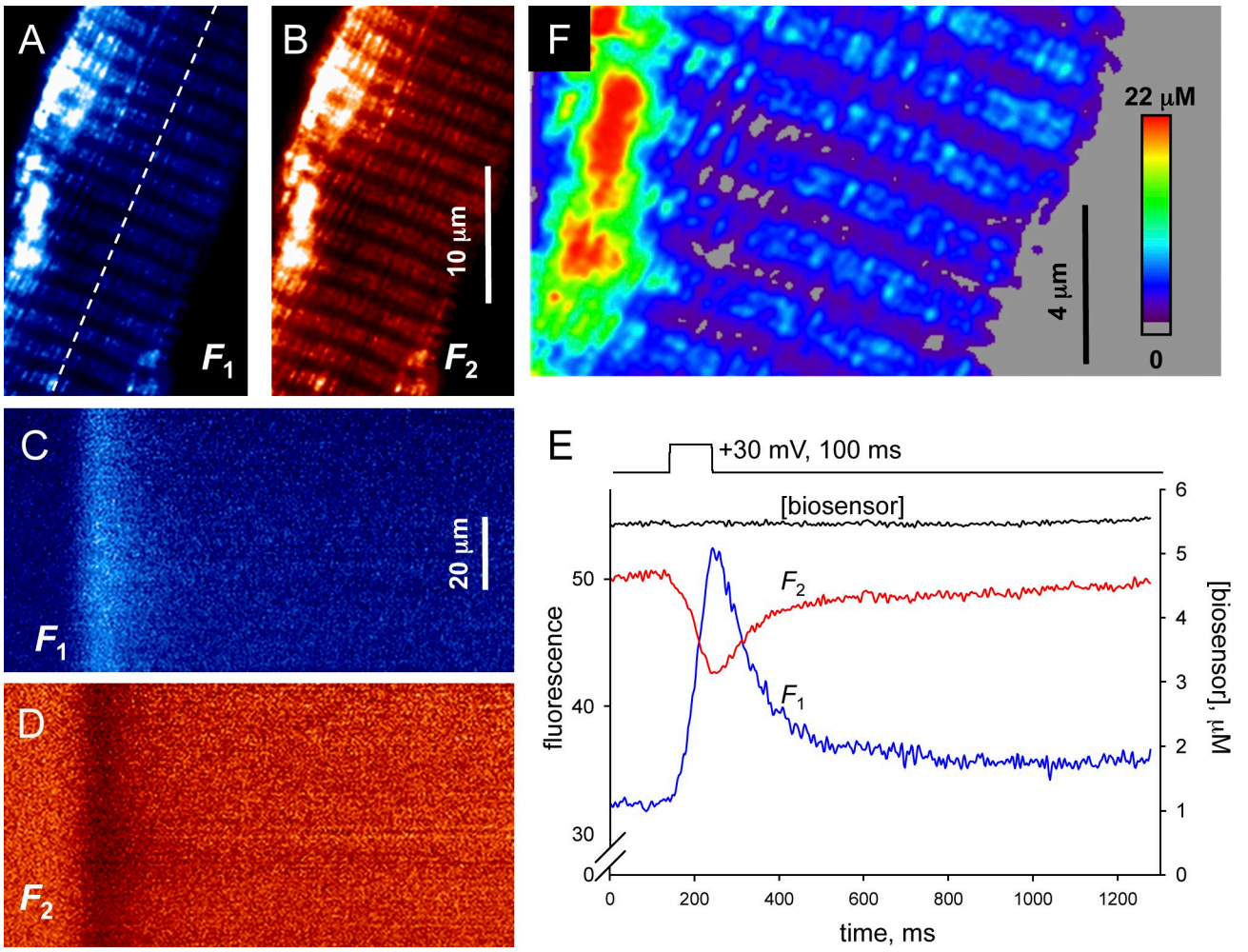

Figure 2. Components of the FRET signal and determination of biosensor concentration. (A and B) "FRET pair" of images obtained simultaneously of a cell expressing D4cpv-Casq1, under voltage control by whole-cell patch. The excitation wavelength was 458 nm. Image $F_1(x,y)$ (or "donor") was collected between 470 and 510 nm; $F_2(x,y)$ between 520 and 580 nm. (C and D) FRET pair, $F_1(x,t)$, $F_2(x,t)$, of line-scan images of fluorescence in the same cell. Calcium release was elicited by the large depolarizing pulse represented in E. (E) Spatially averaged fluorescence $F_1(t)$ (blue) and $F_2(t)$ (red). The black line, which plots biosensor concentration S_T calculated from $F_1(t)$ and $F_2(t)$ using Eq. A6, demonstrates the property of invariance of the measure thus calculated, even when the signals used in the calculation are changing rapidly. (F) Image of biosensor concentration, formed by combining images A and B according to Eq. A6. ID: 082009a series 36 and 39.

Fig. 4 (C and D) shows fluorescence in an analogous experiment on a cell expressing D1ER. The content of the intact cell was 0.39 au, and it was reduced to 0.25 au 1 min after exposure to saponin for 4 min, a 38% reduction. On average, the content was reduced by 29% (SEM 8%; 7 cells). We conclude that little if any D4cpv was expressed outside organelles, but a substantial amount of D1ER was either in the cytosol or bound with low affinity to sites accessible from the cytosol.

TABLE I

Expression of two biosensors in different mouse strains

Strain	Average	SEM	Cells
	μM	μM	n
D4cpv-Casq1 BS	2.9294	0.2551	39
D4cpv-Casq1 SW	1.2418	0.1969	34
D4cpv-δAsp SW	1.6472	0.1379	96

Biosensor concentration was calculated by first constructing the invariant images from F_1 and F_2 using Eq. A6 (as illustrated with Fig. 2), then calculating an image average. Numbers listed are equal weight averages of image averages over n cells. Units are micromoles/liter of fiber. The difference in expression of the two fusion variants, examined in the SW strain, was of moderate significance ($P < 0.10$).

Published July 25, 2011

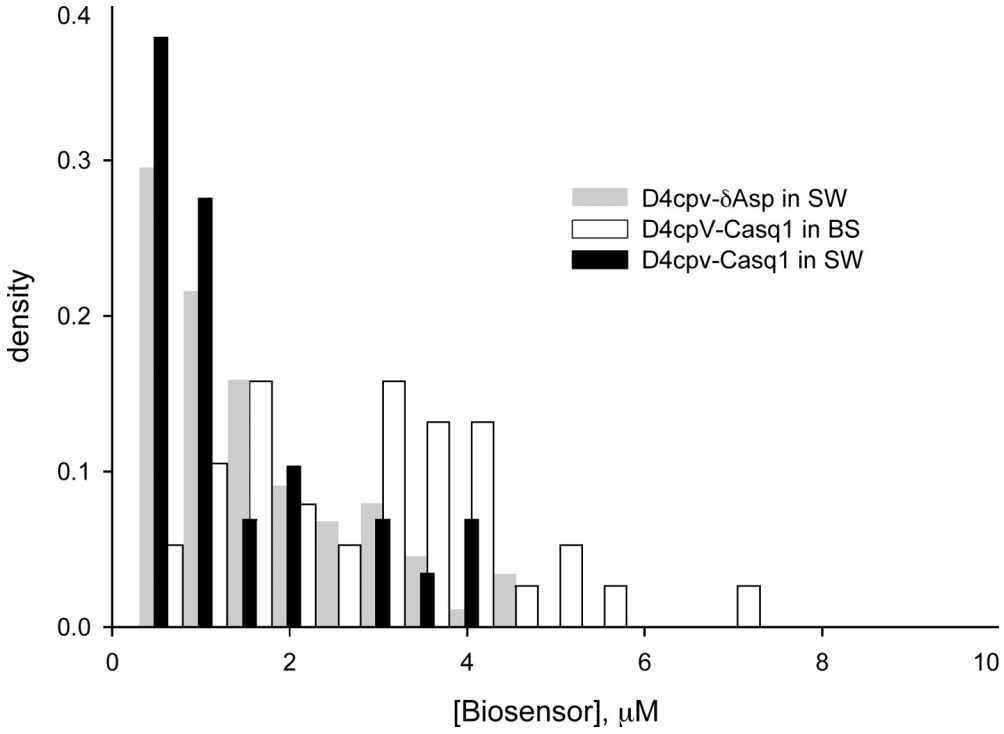

Figure 3. The expression of biosensor under multiple conditions. Histograms of biosensor concentration (in terms of accessible cell volume) calculated by Eq. A6 for the two molecular variants used in this paper. White bars: distribution of concentrations of D4cpv-Casq1, in cells of BS mice. These experiments were done before 7 January 2010, when the deletion variant of the biosensor was not available. Black and gray bars: concentrations of D4cpv-Casq1 and D4cpv-δAsp, compared in the SW strain. Statistical features of the samples, given in Table I, demonstrate a significant difference between the samples in both murine strains. The deletion variant expressed somewhat better than the full clone, at a moderate significance level ($P < 0.10$).

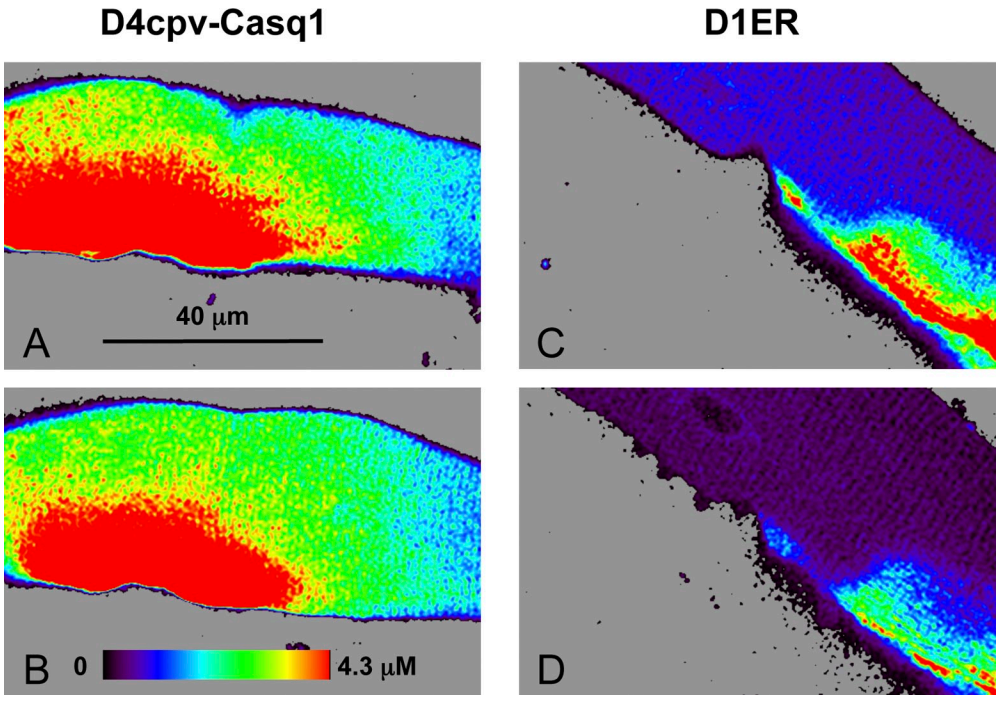

Figure 4. D4cpv-Casq1 and D1ER leave permeabilized cells at different rates. (A) Biosensor concentration in a resting cell expressing D4cpv-Casq1, calculated pixel-by-pixel from images $F_1(x,y)$ and $F_2(x,t)$ by Eq. A6. The cell was exposed later to saponin-containing solution for 4 min. (B) [biosensor] 6 min after the end of the exposure. Image-averaged [biosensor] decreased from 3.11 μM in A to 2.90 μM in B. A calculation in the text shows that the decrease was probably not caused by loss of biosensor from the cell. ID: 062410c images 10 and 12. (C) Image of a cell expressing D1ER at rest. (D) The same cell after identical exposure to saponin. [biosensor] decreased from 0.35 to 0.18 μM. After integration in the volume of the cell, biosensor content decreased from 0.39 to 0.25 au. Note two areas with different concentration and sharp transition in C and D, in contrast with smooth gradient in A and B. ID: 020911d images 82 and 84.

Published July 25, 2011

Calibration of the biosensor signal in cells

Earlier attempts to calibrate cameleon D1ER in mouse muscle found a large variability in results (Rudolf et al., 2006; Canato et al., 2010; Jiménez-Moreno et al., 2010). Our attempts with D1ER, which consisted of the application of a "depletion cocktail" that should bring the FRET ratio of biosensor inside the SR close to R_{min}, yielded decreases in R by up to 0.6, or ~30% of the initial value in the cell at rest. One example is illustrated in Fig. S5. These changes were accompanied by variation in initial and final R values within a similar range, which made their quantitative interpretation difficult. By comparison, and as will be shown below with specific examples, the dynamic range of D4cpv and its fusions was three to four times greater. In view of these results, plus the problems reported in previous work with D1ER and the apparent presence of D1ER in the myoplasm, we concentrated our efforts on the use of D4cpv-X. Because reproducibility of results has been a concern with all cameleons, the calibration measurements with D4cpV-X were performed in multiple ways. A chief purpose in the design of D4cpv was to reduce interference by endogenous ligands of calmodulin (Palmer et al., 2006). In this regard, an additional goal of our study was to characterize variation in biosensor performance within or between cells.

A first set of calibrations was done by permeabilizing the SR membrane to Ca^{2+} in the presence of a solution of known $[Ca^{2+}]$. This was done largely on patched cells, both because the dynamic responses to depolarization could then be evaluated based on a same-cell calibration and because the patch electrode stabilized the cell mechanically throughout the procedure. The plasma membrane was first permeabilized with saponin; then the solution was replaced by one containing 10 µM ionomycin and a known $[Ca^{2+}]$ in the 0 –100 µM range. Finally a solution with high $[Ca^{2+}]$ (1–10 mM) was applied. One example is in Fig. 5, which shows ratio images ($R(x,y) \equiv F_2(x,y)/F_1(x,y)$) of the cell in three stages of the process, and the corresponding distributions of R values in individual pixels. These distributions were well fit by Gaussian functions. In subsequent analysis, the Gaussian mean (R_m, or R when the meaning is clear) was used instead of the average, which can be skewed by small regions with large deviation.

R_m values, calculated in a large number of calibration experiments, are plotted versus applied cytosolic $[Ca^{2+}]$ in Fig. 6 (closed black circles). The best fit with Eq. 2 and the stoichiometry parameter $n = 1$, represented by the dashed curve in black (Fig. 6), has parameter values given in the figure legend. With $n = 1$, Eq. 2 describes single-site one-to-one binding. When n was allowed to vary, the standard error of fit decreased. The standard error of estimate for n, however, was large, and the improvement did not justify the additional parameter (according to the likelihood-ratio test; Bickel and Doksum, 1977).

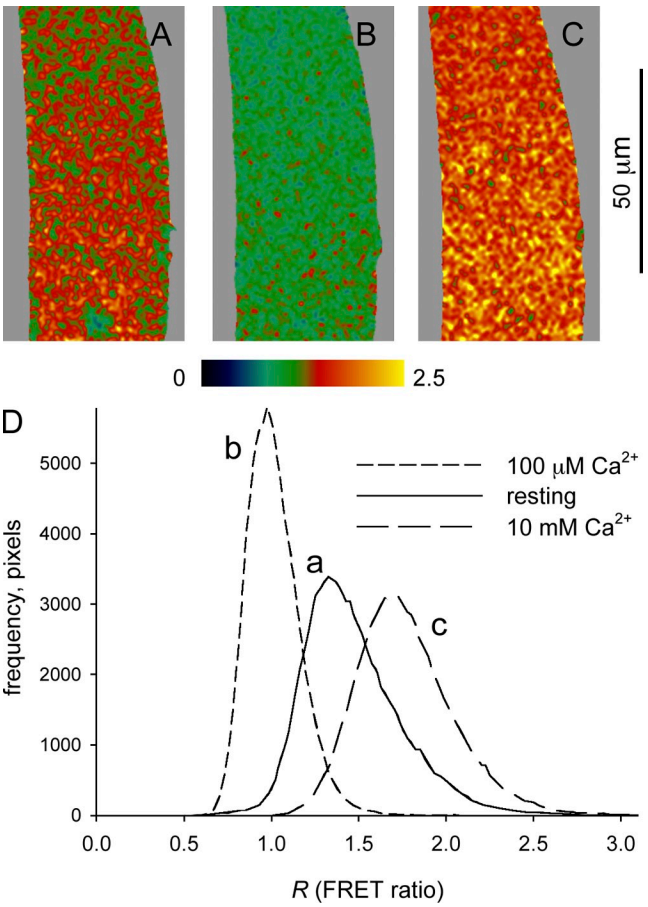

Figure 5. Calibration of the biosensor in cells. (A) A cell expressing D4cpv-Casq1, membrane-permeabilized and immersed in an internal solution with 100 nM $[Ca^{2+}]$. The histogram of FRET ratio, calculated pixel by pixel from A, is curve a in D. R_m, its mean in a Gauss fit, is 1.40. (B) The same cell after permeabilization by saponin and exposure to ionomycin, in the presence of 100 µM $[Ca^{2+}]$. The histogram of R is curve b in D; R_m is 0.97. (C) The same fiber exposed to 10 mM $[Ca^{2+}]$. R_m (from curve c in D) increased to 1.73. The biosensor content calculated from the images was, respectively, 1.31, 1.40, and 1.53, which indicates no loss of biosensor after membrane permeabilization. ID: 08110c, images 24, 26 and 33.

Other calibration methods used are illustrated in Fig. 7. Fig. 7 (A and B) are $R(x,y)$ of an intact cell expressing D4cpv-Casq1, before and after the application of a depleting cocktail. R_m of Fig. 7 B was 0.47, and in 10 similarly prepared cells it was consistently close to the parameter R_{min} fitted to the ionomycin data. Values obtained thus are represented by green circles in Fig. 6 at abscissa 0.1 µM. The inset in Fig. 7 B is a partial view of the image of biosensor concentration, derived as described for Fig. 2, in an expanded scale. The other insets are also partial images of biosensor concentration.

In a third approach, cells were induced to express the biosensor not fused to calsequestrin. D4cpv remained largely in the cytosol, as indicated by the lack of structure in the fluorescence image and a consistently

Published July 25, 2011

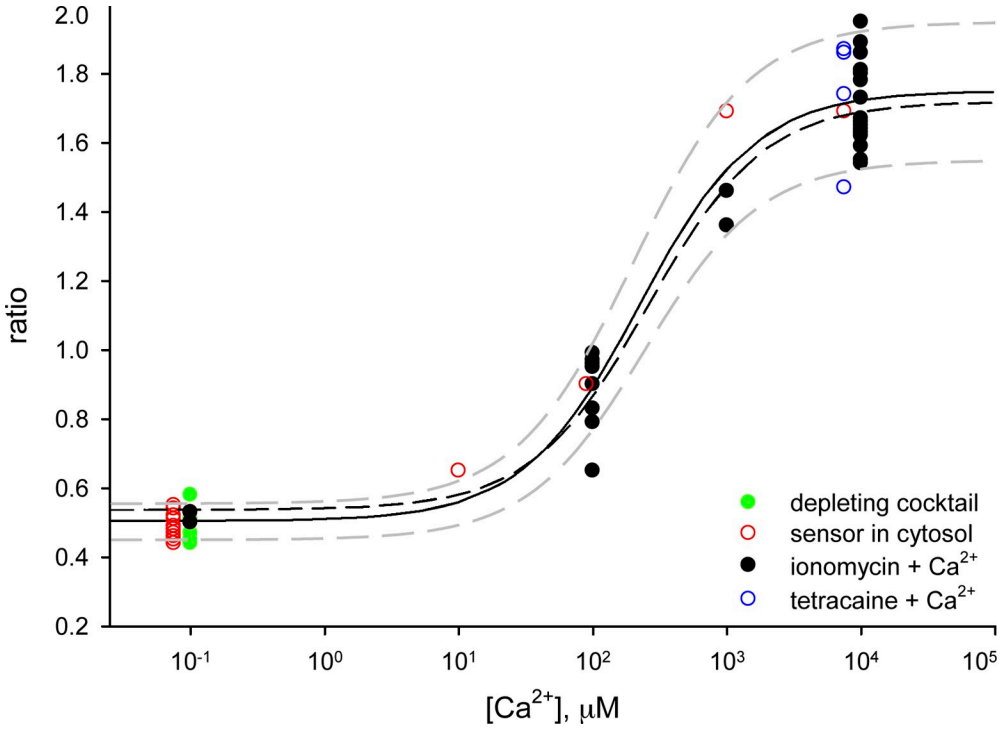

Figure 6. Summary of calibration studies. Black circles, R values obtained in calibrations using 23 fibers permeabilized by saponin and ionomycin and immersed in a solution with the $[Ca^{2+}]$ represented in the abscissa. Up to three data points at different abscissa were obtained for each cell. Green circles, R_m at ~5 min after application of the depletion cocktail described in Materials and methods to nine cells, six of which were intact and three of which were membrane-permeabilized and immersed in a standard, 100 nM $[Ca^{2+}]$ internal solution. All points are plotted at abscissa 100 nM. R_m increased slightly after a minimum reached at ~5 min after application of the cocktail. The minimum was plotted in every case. Red circles, R_m in 15 cells expressing D4cpv, not fused to calsequestrin. 10 of those were membrane permeabilized in a 100 nM $[Ca^{2+}]$ internal solution. In those cells, R_m was not significantly changed after permeabilization. In five other cells R_m measured in solutions with greater $[Ca^{2+}]$ had values also represented by red circles, at the corresponding abscissa. Blue circles, R_m in cells permeabilized by saponin and immersed in a solution with 1 mM tetracaine and 1 μM Ca^{2+} (the 7.5 mM abscissa is justified in the text). The dashed line in black represents the best fit by Eq. 2 with $n = 1$ to the values obtained with the ionomycin technique. Its parameter values are β K_D = 258 μM, R_{min} = 0.53, R_{max} = 1.72. In a continuous line is the best fit to all points, except those obtained in cells exposed to tetracaine. This fit identified the standard values of parameters used to calculate $[Ca^{2+}]_{SR}$ in the present work and its companion paper (Sztretye et al., 2011), namely β K_D = 222 μM, R_{min} = 0.505, R_{max} = 1.74 ($n = 1$). The gray broken lines represent fits at the limit parameter values considered likely (as justified in the Discussion), namely β K_D = 200 μM, R_{min} = 0.555, R_{max} = 1.91 (top curve), or β K_D = 244 μM, R_{min} = 0.455, R_{max} = 1.57 (bottom curve).

low R in cells at rest. Fig. 7 C is a ratio image of a representative cell expressing the unfused sensor. There, R_m is 0.47, which is consistent with an essentially Ca^{2+}-free biosensor. In Fig. 7 D is an image of the same cell after permeabilization with saponin and exposure to a solution with 1 mM free $[Ca^{2+}]$. R_m increased to 1.61. The approach yielded multiple values at resting cytosolic $[Ca^{2+}]$, all of which were close to R_{min} evaluated with ionomycin. The technique was also used in permeabilized cells to characterize the response of the unfused biosensor to different $[Ca^{2+}]$. The approach was hampered, however, by the eventual loss of biosensor through the plasma membrane. R_m values obtained with this approach are represented by red circles in Fig. 6.

Fig. 7 (E and F) illustrates an intervention that yielded large elevations of R_m, which is consistent with a saturating increase in $[Ca^{2+}]_{SR}$. Fig. 7 E has the R image of a resting cell transfected with D4cpv-Casq1. F shows R in the same cell after saponin permeabilization and exposure to an internal solution containing 0.5 mM tetracaine and 1 μM $[Ca^{2+}]$. R_m in this example increased from 1.28 to 1.81 (a value greater than R_{max} of the best fit to all data). Mean ratios in cells exposed to tetracaine plus elevated $[Ca^{2+}]_{cyto}$ are represented in Fig. 6 by open blue circles, arbitrarily plotted at abscissa 7,500 μM (the actual $[Ca^{2+}]_{SR}$ being in the saturating range and therefore unknown).

The R values attained by these manipulations can be collectively described by a single dependence on $[Ca^{2+}]$. The solid curve in Fig. 6 represents the best fit of Eq. 2 to all points (excluding the data in tetracaine, for which the actual abscissa is unknown). The best fit parameters (R_{min} = 0.505, R_{max} = 1.74, and βK_d = 222 μM) were used with Eq. 1 to calculate $[Ca^{2+}]_{SR}$ in subsequent analyses. In Fig. 6, the broken gray lines, generated as described in the figure legend and justified in the Discussion, represent confidence limits for the calibration. β was directly measured in two cells with SR permeabilized by ionomycin and exposed sequentially to 0 and 10 mM $[Ca^{2+}]$, and in one cell expressing D4cpv alone when it was intact and after membrane permeabilization and exposure to 10 mM $[Ca^{2+}]$, as the ratio of F_1 in the two solutions (Materials and methods). The average of three determinations was 0.554 (SEM = 0.017).

An additional set of calibration measurements was conducted on D4cpv protein, biosynthesized and purified in our laboratory. The protein was shown to be pure by conventional chromatography and also because

Published July 25, 2011

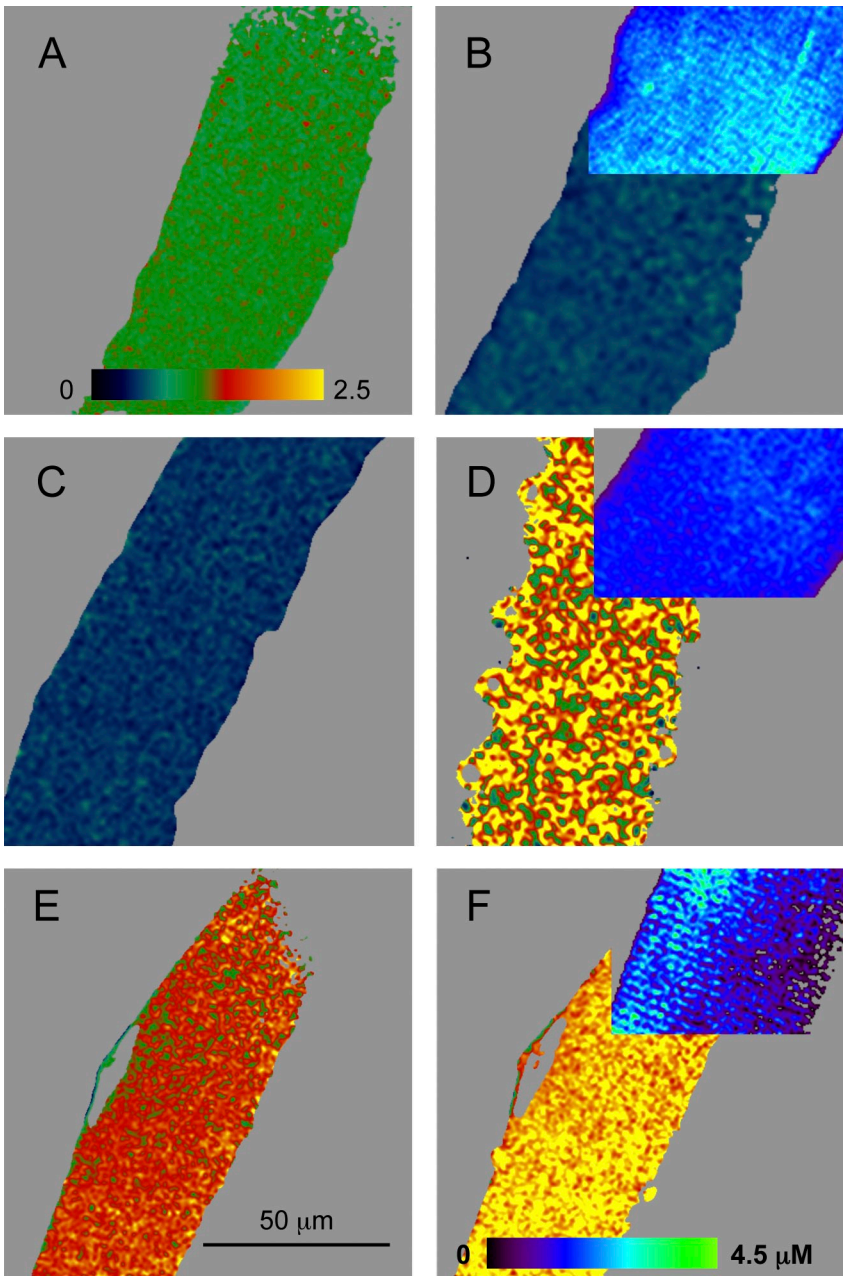

Figure 7. Alternative calibration methods. (A) $R(x,y)$ in an intact cell at rest. (B) The same cell after 2 min in a depletion cocktail. ID: 052809a images 14 and 18. (C) $R(x,y)$ in a cell expressing D4cpv (untargeted). (D) The same cell after membrane permeabilization and immersion in internal solution with 1 mM [Ca^{2+}]. ID: 041509g images 3 and 13. (E) $R(x,y)$ in an intact cell at rest. (F) The same cell, after membrane permeabilization and exposure (for 20 min) to a solution containing 1 μM free[Ca^{2+}] and 1 mM tetracaine. ID: 060409b images 67 and 82. The color table for R is in A; the table for [biosensor] is shown in F. Gaussian means R_m for all images are given in the text. Partial images of biosensor concentration, computed from the same data, are presented in insets at a scale enlarged 1.5 times. All images were obtained at low spatial resolution, but they still show comparative lack of structure in inset D for the cell expressing untargeted D4cpv.

the molarities of the two fluorophores, measured by absorption spectrometry, were within 10% of each other. Fluorescence F_1 and F_2 of solutions of 3 μM of this protein in the presence of 0 or 10 mM [Ca^{2+}] were imaged in small coverslip chambers, with the same confocal microscope settings used for cells. The average of R_m over 10 separate measurements, 0.3500 (SEM = 0.007) and 1.49 (SEM = 0.042) were significantly lower than R_{min} and R_{max} evaluated in cells. The dynamic range instead was similar to that determined in calibrations inside cells. We do not have a preferred explanation for this shift to lower values of R. That the solutions were made with the biosensor protein rather than its fusion with Casq1 does not explain the shift, because unfused D4cpv expressed in the cytosol had a similar response to Ca^{2+} as calsequestrin-fused biosensor in the SR.

A limited evaluation of the response of D1ER in our setup was performed by applying the depletion cocktail to resting cells expressing D1ER. An example experiment is illustrated in the supplemental materials. In four cells of four mice, resting R was 1.79 (SEM = 0.10) and the depletion cocktail caused a reduction to 1.39 (SEM = 0.02) after Ca^{2+} release.

High-expression areas had a lower FRET ratio

A slight spatial variation in R with biosensor concentration was observed in most cells. In 45 out of 68 cells

Published July 25, 2011

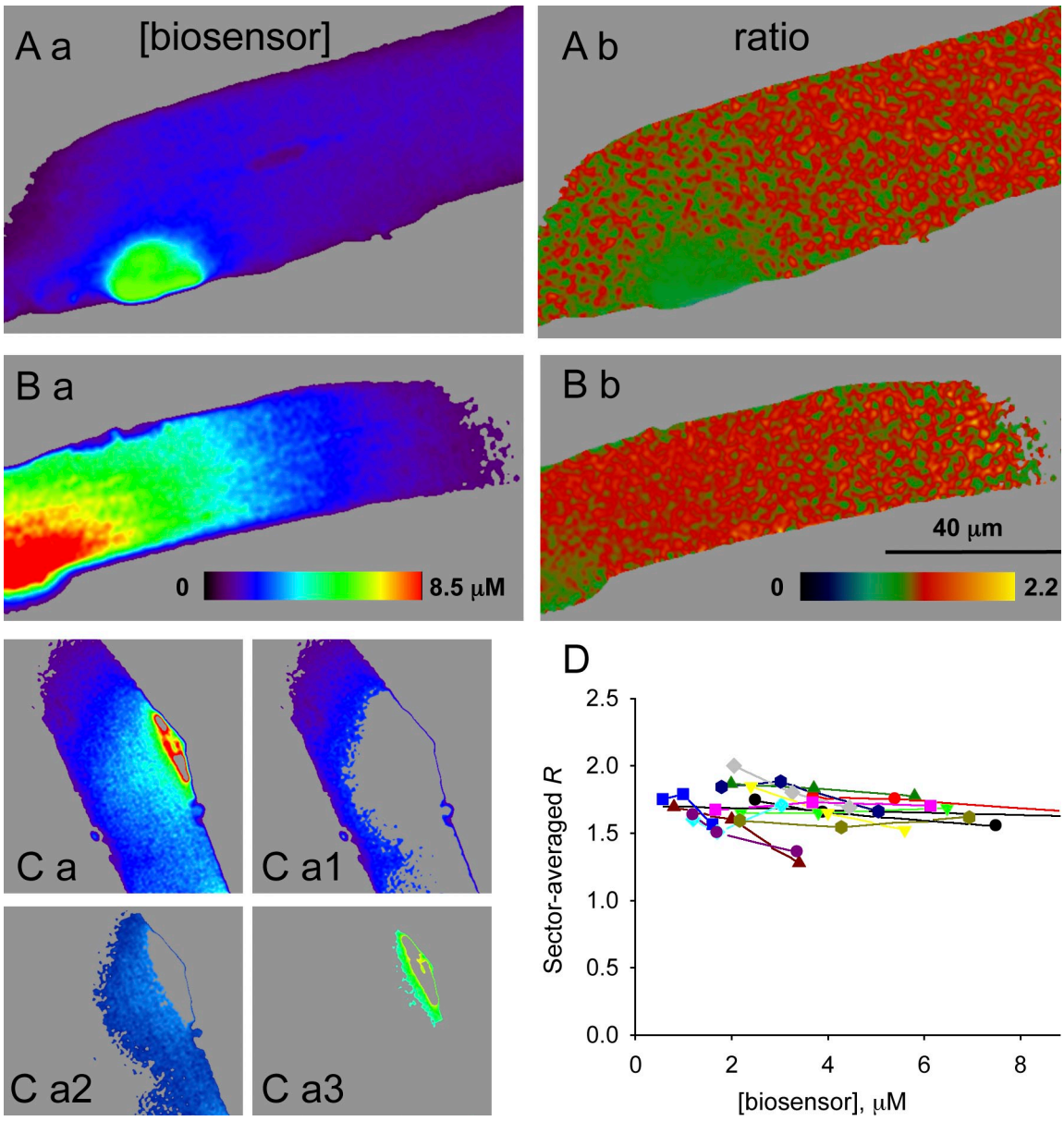

Figure 8. Biosensor concentration and FRET ratio. "a" panels show biosensor concentration calculated by Eq. A6. "b" panels show FRET ratio *R*. (A) A cell showing substantial variation of *R* with biosensor concentration (maroon circles in summary plot D). (B) An example with homogeneous *R* values, in spite of large gradients in biosensor concentration (pink squares in D). (C) A cell with moderate change of *R* with [biosensor] (black circles in D). (C, a1–a3) Sectors of increasing [biosensor], averaging, respectively, 1.79, 3.02, and 5.05 μM. In this example, like in every cell, areas of lower biosensor concentration were increasingly farther from transcribing nuclei. (D) Sector-restricted R_m versus sector-averaged [biosensor] in 12 cells at saturating or near-saturating $[Ca^{2+}]_{SR}$. Different cells are represented by different symbols. In every case, the cell image is separated in three nonoverlapping sectors of increasing [biosensor]. Note that in most cells, R_m decreases slightly with [biosensor], but there is no such correlation across different cells. See text for further details. ID: A, 070710a image 36; B, 072309a image 29; C, 060409b image 67.

with D4cpv-X, areas of greater expression tended to have a slightly lower ratio value. Because this dependence could help explain some variability found in calibrations of D1ER and D4cpv, we explored it further.

A similar dependence of *R* with biosensor concentration was found for both biosensor variants. It applied to resting cells as well as cells with plasma membrane permeabilized, and in conditions that impose a high $[Ca^{2+}]_{SR}$ (described above in the Calibration section). Images of three cells under such conditions are shown in Fig. 8. In Fig. 8, images labeled a are colorized by the concentration of biosensor and images labeled b are colorized by the *R* value. It can be seen that in the regions of higher [biosensor], the ratio was slightly lower for cell A but not substantially different for cell B.

Published July 25, 2011

We quantified this effect in 12 cells expressing D4cpv-Casq1 by dividing the image of the cell in three disjoint sectors of low, intermediate, and high biosensor concentration (the sector limits were determined individually for each cell, in terms of standard deviations from a mean value of biosensor concentration). Such sectorization is illustrated in the figure for cell C (Fig. 8). Fig. 8 C (a) presents [biosensor] in the full image, whereas Fig. 8 C (a1, a2, and a3) shows the three sectors in increasing order of biosensor concentration. The sector average of R is plotted versus the average [biosensor] for different cells in Fig. 8 D. A negative correlation between the variables was found in 9 of 12 cells. In those, the value of R was 3–15% less in the third than in the first sector. As can be seen by inspection of the graph, the correlation was equally present in cells with low or high average [biosensor]. When all cells were taken into account, there was no correlation between cell-averaged R and [biosensor] (the correlation coefficient ρ^2 was −0.03 for all points in the graph).

Because the variation of R with [D4cpv] is present in conditions of biosensor saturation as well as in cells at rest, the differences must reflect local variations in performance of the biosensor, rather than changes in $[Ca^{2+}]_{SR}$. Because the heterogeneity is equally visible in cells with vastly different levels of expression, the greater R in regions where [D4cpv-X] is lower is probably not determined by the local [D4cpv-X]. In every case, the relative concentration of the biosensor decreases as the distance from actively transcribing nuclei (and perinuclear areas of protein synthesis) increases. Therefore (and as clearly seen in the illustration), the relative concentration of biosensor constitutes a proxy for distance from the site of synthesis (and time since synthesis). These features suggest a likely explanation for the observed gradient in FRET ratio: a posttranslational modification, a "maturation" of the biosensor, which takes time and progresses as the sensor migrates away from the sites of synthesis. The functional difference is small. It is, however, objectively demonstrated, and constitutes a likely cause of the relative dispersion in calibration measurements, as well as aspects of the resting $[Ca^{2+}]_{SR}$ described in the next section.

Resting SR calcium concentration

$[Ca^{2+}]_{SR}$ of resting cells, expressing D4cpv-Casq1 and quiescent in "external" solution, was derived from their R_m using Eq. 1 with the parameter values defined in the previous section. The functional response of all cells was later studied under patch voltage clamp, with X-rhod-1 in the pipette. Their cytosolic Ca^{2+} transients were recorded and analyzed as illustrated in the companion paper (Sztretye et al., 2011). To discard cells affected by the enzymatic dissociation, data were included only for cells that, visually, and by electrophysiological and other functional criteria, appeared not to be damaged.

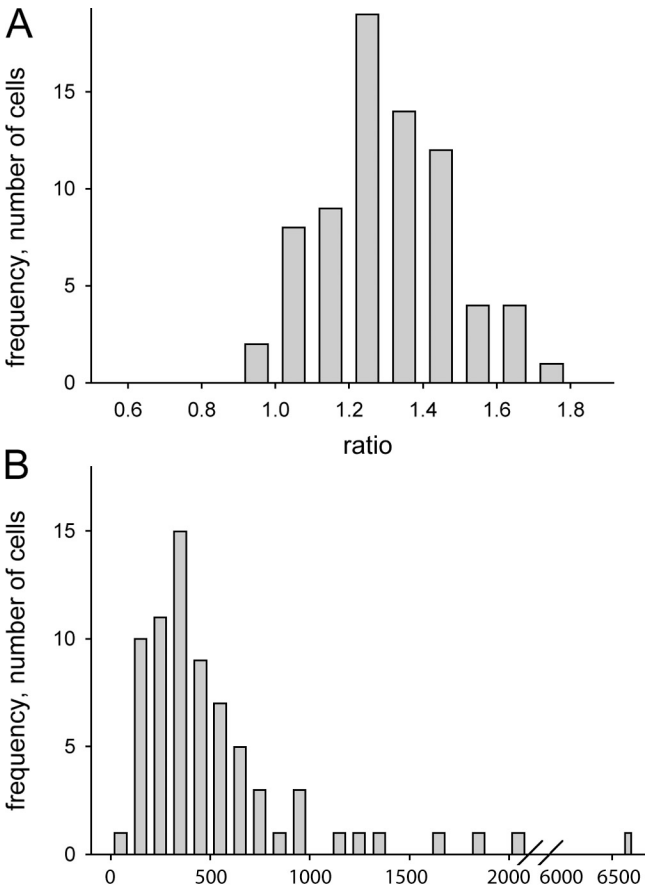

Figure 9. FRET ratio and $[Ca^{2+}]_{SR}$ in resting cells. (A) Histogram of R_m in 74 cells (61 expressing D4cpv-Casq1 and 13 expressing D4cpv-δAsp), immersed while intact in "external" solution and later vetted as described in the text. (B) Histogram of $[Ca^{2+}]_{SR}$ calculated individually from R_m values in A, using Eq. 1 with parameters determined in cells as illustrated in Fig. 6. Note the marked asymmetry of the distribution.

This meant that they could be patched and held at −80 mV with limited holding current, assuming linear membrane capacitance did not increase significantly for at least 30 min, and yielded spatially homogeneous cytosolic Ca^{2+} transients (indicative of a fast and homogeneous voltage clamp). These criteria were purposely broad so that cells with variable SR loads could be included in the measurements. 74 cells from 25 mice satisfied the criteria; 61 expressed D4cpv-Casq1 and 13 expressed D4cpv-δAsp. The histogram of R_m measured in individual cells before patching is represented in Fig. 9 A. The histogram was consistent with a Gaussian distribution. Mean R_m was 1.31 (SEM = 0.02). The average did not depend on the biosensor variant: 1.32 (SEM = 0.03) for D4cpv-Casq1 and 1.28 (SEM = 0.04) for D4cpv-δAsp.

$[Ca^{2+}]_{SR}$ values were calculated from individual R_m; their histogram is plotted in Fig. 9 B. As shown, $[Ca^{2+}]_{SR}$ varied in a very wide range. The distribution of resting $[Ca^{2+}]_{SR}$ was skewed, including several cells with concentration >1 mM.

Published July 25, 2011

As elaborated in the Discussion, this asymmetry is satisfactorily explained by a small cell-to-cell variation of the biosensor parameters.

Because of the skewness of the distribution of concentrations, their average (614 µM) is a poor representation of the central tendency. More representative are $[Ca^{2+}]$ calculated from the average R_m (415 µM), or the median, 374 µM.

DISCUSSION

The present results demonstrate the use of a novel biosensor targeted to the SR, made by fusion of calsequestrin 1 or a deletion variant of the same protein, and cameleon D4cpv (Palmer et al., 2006).

The novel biosensor exhibits a desirable localization at terminal cisternae

D4cpv-X expresses in a highly localized manner, residing in what is identified as SR terminal cisternae, based on the similarity of images of biosensor fluorescence and anti-Casq1 immunofluorescence. The distribution and retention of the biosensor were consistent with the expectations for a fusion protein that includes calsequestrin, which is highly specifically targeted to the SR.

D1ER featured clear differences in the spatial patterns of expression, documented in the supplemental materials. Fully understanding the implications of these differences is well beyond the scope and purpose of the present work. In an initial evaluation, D4cpv fusions appear superior for several reasons. One is their clear placement at terminal cisternae, indicated by colocalization with t tubules, in contrast with the more widespread distribution of D1ER. The presence of D4cpv in terminal cisternae confers it some kinetic advantage given the small but measurable delay in the evolution of $[Ca^{2+}]$ expected between longitudinal SR and terminal cisternae (Pape et al., 2007).

A more compelling reason to prefer the calsequestrin-fused D4cpv to D1ER is its superior retention in membrane-permeabilized cells. The average 29% loss of the D1ER content after 10 minutes in cells exposed to saponin suggests that part of D1ER is in the myoplasm, in solution or loosely bound to structures accessible from the cytosol. Considering that the targeting of D1ER is accomplished by the retention/retrieval and signal sequences of calreticulin, the distribution of D1ER is consistent with evidence of the presence of calreticulin in cytosol and nuclei of various types of cells (Holaska et al., 2001; Afshar et al., 2005), which was found in search of explanations for reported roles of calreticulin in cytosol and nuclei (e.g., Rojiani et al., 1991; Dedhar et al., 1994; for review see Dedhar, 1994).

Additional reasons to prefer D4cpv-X relate to its monitoring function, and are discussed in the next subsection.

The distribution of D4cpv-X within the cell varied widely. Expressed in terms of the cell volume, the concentration of biosensor reached up to 22 µM in perinuclear regions, but a typical cell-averaged value was 2 µM. Considering that the SR occupies 5.5% of cell volume in the mouse, the actual concentration of expressed biosensor might reach 22/0.055, or 400 µmoles/liter of SR. Assuming that every calsequestrin molecule provides 80 sites for Ca^{2+}, the biosensor would typically contribute 160 µmoles of additional Ca^{2+}-binding sites per liter of fiber. This amounts to ~4% of the maximal calcium content of rat muscle (3.85 mmoles per liter of fiber; Fryer and Stephenson 1996) or 5.5% of the calcium binding sites associated to calsequestrin in fast twitch rat muscle (Murphy et al., 2009).

The biosensor can be uniformly calibrated within cells.

As illustrated in Fig. 6, the dependence $R([Ca^{2+}])$ observed under calibration conditions established by various methods was collectively fit by the conventional one-site binding function (Eq. 2). A crucial figure of merit is the dynamic range, defined here for ratiometric sensors as $DR \equiv (R_{max} - R_{min})/R_{min}$. DR is proportional to the magnitude of the signal, which in turn determines the sensitivity and signal/noise ratio. For D4cpv-X, it was $(1.74 - 0.505)/0.505$, or 2.45, slightly less than the 3.0 measured for D4cpv alone in vitro (Palmer et al., 2006), which is probably because we used a different excitation wavelength and consequently had to collected emitted light over different wavelength ranges. The fitted value of βK_d, 222 µM, divided by the directly measured β yields K_d = 401 µM. This is greater than the value reported for D4cpv in solution (65 µM; Palmer et al., 2006), a common observation with other monitors, including D1ER (Rudolf et al., 2006). Considering that βK_d is equal to the $[Ca^{2+}]$ of half-signal, the sensitivity of D4cpv turns out to be excessive for the measurement of $[Ca^{2+}]_{SR}$. Monitors with this sensitivity cannot follow situations of calcium overload, as clearly demonstrated by the observations in cells exposed to elevated $[Ca^{2+}]_{cyto}$ and tetracaine, which yielded R values consistently close to R_{max}.

For evaluation of D4cpv, it is useful to compare its DR with that found for D1ER. In a calibration in situ by Canato et al. (2010; Fig. S2), R decreased from 1.89 to 1.51 in a cell exposed to a depleting solution. Equating R_{max} to the highest R value recorded, 2.4, the calculated DR is 0.59. In the work of Rudolf et al. (2006; Fig. S2 C), R_{min} is 2.3 and R_{max} is 4.2, for a DR of 0.83. In our own limited testing, an example of which is in Fig. S5, R_{min} was 1.39 and the maximum value of R observed in 12 cells was 2.50, for a DR equal to 0.80. In these practical assessments, DR of D4cpv-Casq1 is therefore three to four times greater than that of D1ER, which confirms the differences reported for the sensors in solution (Palmer et al., 2006). In agreement with the calibrations, examples

Published July 25, 2011

in the companion paper (Sztretye et al., 2011) will show decreases of R in cells subjected to depleting depolarizing pulses of magnitude $[(R\text{-}R_{min})/R_{min}]$ up to 1.8, a value much greater than comparative measures in the studies with D1ER.

Calibrations of D4cpv (not fused with calsequestrin) biosynthesized in the laboratory yielded significantly lower R_{min} and R_{max}. Several reasons for this difference were ruled out. The presence of incomplete biosensor would result in an excess of donor fluorophore, which in turn would have reduced both R_{max} and R_{min}. This is in agreement with the observations, but would also have reduced the dynamic range of the signal, which was not the case. An "immature" or imperfectly folded protein would have also had a lower dynamic range. Differences attributable to the fusion of calsequestrin were unlikely because unfused D4cpv expressed in the cytosol yielded approximately the same R values as the full biosensor. We conclude that unknown factors in the cellular environment may change the behavior of the protein in ways that cannot be justified simply, and therefore calibrations in solution cannot substitute for those performed in the cellular environment.

The resting $[Ca^{2+}]_{SR}$ is consistent with earlier estimates with D1ER and Fluo-5N

The value of R, calculated in 74 cells at rest, was distributed approximately normally around a mean of 1.31, a value that translates to an SR calcium concentration of 415 μM. The median of the sample was 374 μM. These values, which were obtained in enzymatically dissociated fibers and therefore are not strictly physiological, are consistent with earlier estimates obtained with D1ER in muscles of live mice (308 μM; Rudolf et al., 2006) or Fluo-5N in enzymatically dissociated cells (391 μM; Ziman et al., 2010). Collectively, these estimates are similar to the average $[Ca^{2+}]_{SR}$ measured in frog muscle cells at $[Ca^{2+}]_{cyto}$ = 100 nM using shifted excitation and emission ratioing (SEER) of Mf mag-indo-1 (Launikonis et al., 2005). They are comparable with values obtained with fura-2 or targeted probes in the ER of various cells, which range from 100 to 600 μM (Golovina and Blaustein, 1997; Demaurex and Frieden, 2003), but lower than the 1–1.5 mM calculated from fluorine nuclear magnetic resonance (NMR) of TF-BAPTA in beating hearts (Chen et al., 1996).

For these various SR probes, the ratio of $[Ca^{2+}]_{SR}$ to $[Ca^{2+}]_{cyto}$ is ∼3,000–4,000. These estimates are far from reaching the ∼75,000-fold maximum ratio predicted by the energetics of the SR Ca^{2+} pump under physiological conditions (e.g., Pickart and Jencks, 1984). An explanation for this difference is seen in Inesi (1994). It invokes a reduction in SR pump turnover rate by lumenal Ca^{2+} (an allosteric inhibition, unrelated to the role of substrate) associated with the increase in $[Ca^{2+}]_{SR}$ beyond 1 or 2 mM. In the presence of leaks through open Ca^{2+} channels and through the pump itself, this inhibition results in stabilization of $[Ca^{2+}]_{SR}$ at values well below the thermodynamic limit. The present measurements therefore join a trend that puts the resting $[Ca^{2+}]_{SR}$ of skeletal muscle at or below 0.5 mM. This number is less than the value, 1 mM, most often assumed in quantitative analyses of currents and fluxes. For example, Kettlun et al. (2003) and Mejía-Alvarez et al. (1999) estimated unitary flux current under "physiologic" conditions as 0.35 to 0.5 pA, from bilayer currents driven by 1 mM $[Ca^{2+}]_{cis}$. With 0.5 mM $[Ca^{2+}]_{cis}$, the estimate would have been reduced approximately by half.

"Noise" in the biosensor skews the distribution of measured $[Ca^{2+}]_{SR}$

As shown by the histogram in Fig. 9 B, the distribution of concentrations calculated from R values of individual cells is asymmetrical, with several individual values greater than 1 mM and one at 6.7 mM. Although it is thermodynamically possible to reach such values, the asymmetry of the distribution suggests an alternative explanation.

Before developing the alternative, an additional problem can be noted: the distribution of R values over multiple cells (Fig. 9 A) is symmetrical, well-fitted by a Gaussian function. The FRET ratio R, however, is a derived quantity, generated by the operation represented by Eq. 2 acting on $[Ca^{2+}]_{SR}$, a random and presumably Gaussian variable.

We will show that both anomalies—the skewed distribution of $[Ca^{2+}]_{SR}$ and the symmetrical distribution of R—have a common explanation. Small errors, either in the measurement of R or the calibration parameters, will result in errors in calculated $[Ca^{2+}]$ that grow disproportionately as the sensor approaches saturation. The nonlinearity arises because according to Eq. 1, $d[Ca^{2+}]/dR$ is inversely proportional to $(R_{max} - R)^2$. Errors therefore become severe when R approaches R_{max}, as is often the case because D4cpv has a low K_d. Because of the symmetrical role of R_{max} and R in $d[Ca^{2+}]/dR$, similar errors in $[Ca^{2+}]$ will be caused by errors in the measurement of R and by changes in R_{max}. This idea is used in a simple simulation to prove that a sample of $[Ca^{2+}]$ with normal distribution will be reported as skewed by a sensor of high affinity and minor variations ("noise") in its parameter values.

The simulation starts by generating a set of 10,000 concentrations with normal distribution around a central value, 400 μM, which is high by comparison with the effective K_d of the hypothetical biosensor (assumed in the simulation to be 222 μM). The histogram of such a set is plotted in Fig.10 A in full trace. Individual concentrations are then operated on by Eq. 2, representing the biosensor, but its three parameters are made to vary randomly, with normal distribution of standard deviation equal to 0.1 of the mean parameter value. Fig. 10 B is the histogram of the set of 10,000 R values generated

Published July 25, 2011

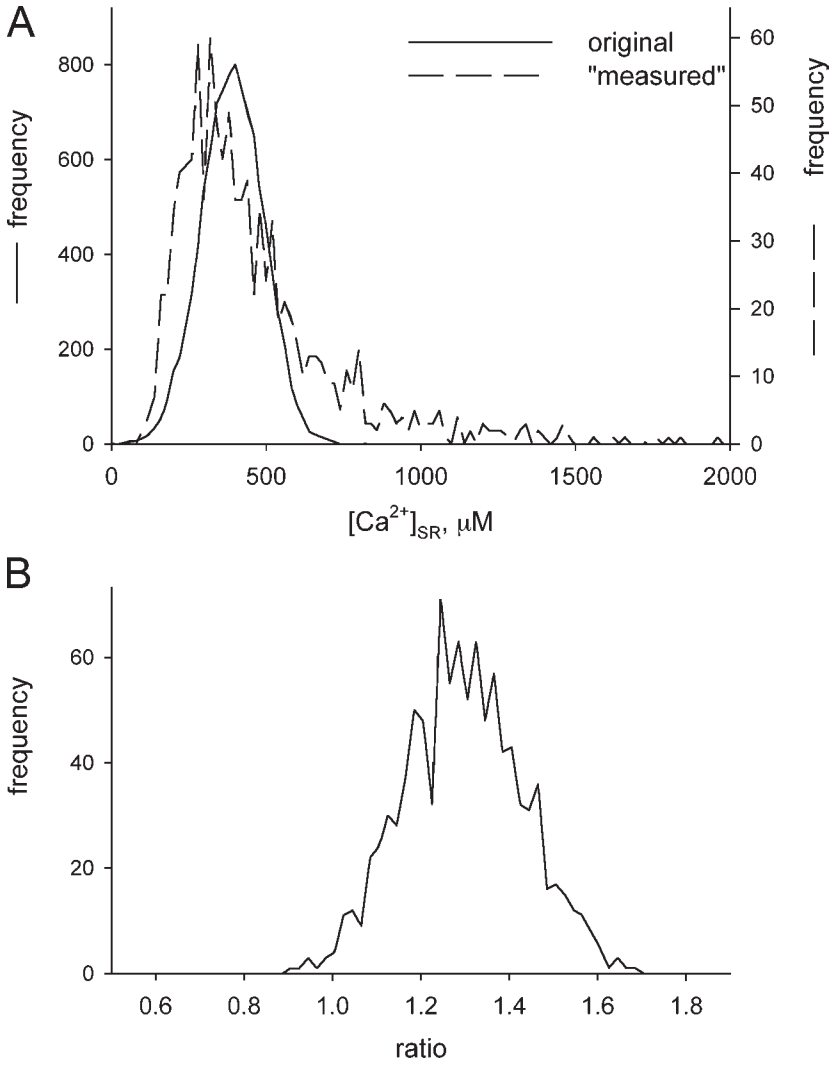

Figure 10. Simulation of a monitor with variable parameters. (A) Continuous trace: histogram of 10,000 $[Ca^{2+}]$ values, randomly distributed according to a Gaussian of mean 400 μM and standard deviation 100 μM. Broken line: distribution of $[Ca^{2+}]$ derived from measurement by a model biosensor as described below. (B) Distribution of *R* values derived from the $[Ca^{2+}]$ values in A with the model biosensor. Individual *R* values were calculated by Eq. 2 operating on the 10,000 individual $[Ca^{2+}]$ using random biosensor parameter values with Gaussian distribution, with the mean equal to their best fit value (β K_d = 222 μM, R_{min} = 0.505, R_{max} = 1.74) and standard deviation equal to 0.1 of said value. The "measured" $[Ca^{2+}]$ values represented in A (broken line) were obtained using Eq. 1 with the best fit parameter values, operating on the *R* values in B. This is a realistic representation of features of the actual biosensor because the histogram of *R* values is similar to the experimental one (Fig. 9 A), and so is the simulated distribution of measured $[Ca^{2+}]_{SR}$ (compared with that in Fig. 9 B).

in this way. Then the set of *R* values is operated by Eq. 1, this time with best-fit parameters, to calculate the "measured" or "reported" $[Ca^{2+}]$. The histogram of reported concentration is plotted back in Fig. 10 A (broken line). This histogram is similar, qualitatively and quantitatively, to the experimental histogram of $[Ca^{2+}]_{SR}$ plotted in Fig. 9 B. Clearly, the simulation reproduces the main features of the observation. We conclude that a small cell-to-cell variation in the properties of the biosensor results in a distribution of FRET ratios that will yield a skewed distribution of reported concentrations if the ratios are interpreted using single-valued parameters. A probable error of 10% in parameter values reproduces well the quantitative aspects of the observed distributions of *R* and $[Ca^{2+}]_{SR}$.

This analysis can also be used to estimate the errors of measurement derived from variations of the monitor as hypothesized in the simulation. Specifically, the average of the population of "measured" $[Ca^{2+}]$ (that is, the average of the histogram in Fig. 10 A, broken line) is 443 μM. An alternative, and somewhat better, use of this hypothetically "noisy" monitor is to calculate $[Ca^{2+}]$ by application of the operator (Eq. 1) to the average value of ratio, 1.281, which yields 376 μM. With either approach, the monitor recovers a value that is close to the true central value in the simulation, 400 μM.

Another reason for the observed variability could be the presence of different fiber types in our samples. The relative frequency of fast (IIA, IIX/D) and slow (I) fibers in FDB is 83 and 17%, respectively (Gonzalez et al., 2003). Type I fibers are located in the deep parts of the muscle (Fig. 3 A; Calderón et al., 2009); therefore, they are underrepresented when the muscle is dissociated enzymatically (outer cells separate in the usual procedure). Therefore, our sample is likely to have a vast majority of fast-twitch cells, and diversity of fiber types may only explain a minor part of the observed variability.

Among available options to measure $[Ca^{2+}]$ inside the SR of mammalian muscle, fluo-5N has provided the fastest signals, whereas D1ER has allowed studies of changes in $[Ca^{2+}]_{SR}$ in a living, working muscle (Rudolf et al., 2006) and revealed unexpected aspects of those changes

Published July 25, 2011

in isolated cells. D4cpv fused with calsequestrin is now found to improve on those monitors. It is expressed abundantly in adult mice. It targeted highly specifically to the terminal cisternae of the SR, at concentrations sufficient to provide a sensitive measure. Calibrated in muscle cells, it displayed a three-to-fourfold greater dynamic range than D1ER. It reported a resting $[Ca^{2+}]_{SR}$ at ~400 μM. Calmodulin-based biosensor properties may vary from cell to cell. This variation, however, appears to be minor in the case of D4cpv, and not affect substantially the central measures of concentration. The potential of D4cpv-Casq1 to refine measurements of dynamic changes in $[Ca^{2+}]_{SR}$ is demonstrated in the companion paper (Sztretye et al., 2011).

APPENDIX

A linear combination of fluorescence intensities proportional to biosensor concentration

The biosensor concentration, S_T, was determined in every cell based on the "invariant" metric first introduced by Launikonis et al. (2005) for the SEER ratioing method. In this appendix, the metric is reintroduced, and adapted to its use to emission ratioing with FRET biosensors.

The well-known advantage of ratiometric sensors is that they yield a number, the ratio, which is related to $[Ca^{2+}]$ independently of S_T. By simple symmetry of the dependence of fluorescence on the two reagents—sensor and Ca^{2+}—a fluorescence metric must exist that is related to S_T independently of $[Ca^{2+}]$. The simplest example is the fluorescence at the isosbestic, isoemission, or crossover wavelength, which is $[Ca^{2+}]$ independent. Even in the absence of an isosbestic signal, a particular linear combination of intensities at two wavelengths exists, which is independent of $[Ca^{2+}]$ and proportional to S_T.

Let e_{D1} be the fluorescence F_1 (collected in range 470–510 nm, the "donor" range) for unit excitation intensity and unit sensor concentration S_T at $[Ca^{2+}] = 0$, e_{C1} the corresponding value in saturating $[Ca^{2+}]$, and e_{D2} and e_{C2} the corresponding F_2 values (in the "acceptor" range 520–580 nm). Then at the $[Ca^{2+}]$ that produces a concentration $[CaS]$ of Ca^{2+}-bound sensor, the fluorescence intensities excited by light of intensity I (in regions far from donor saturation) will be, respectively,

$$F_1 = I\left(S_T e_{D1} + [CaS] e_{C1}\right) \quad \text{and}$$

$$F_2 = I\left(S_T e_{D2} + [CaS] e_{C2}\right) \tag{A1}$$

It is possible to find a factor M so that

$$F_1 + MF_2 = \kappa I\left(S_T + [CaS]\right) \tag{A2}$$

at any $[Ca^{2+}]$ (κ is a constant). Launikonis et al. (2005) called $F_1 + M F_2$ the "invariant linear combination."

Eq. A2 can be solved for M by substituting F_1 and F_2 from Eq. 1:

$$I\left(S_T e_{D1} + [CaS] e_{C1} + MS_T e_{D2} + M[CaS] e_{C2}\right) = I\kappa\left(S_T + [CaS]\right). \tag{A3}$$

Eq. A3 can only be satisfied in general if it is separately true for S_T and $[CaS]$. From these equalities, two expressions for κ result, which yield

$$M = \left(e_{D1} - e_{C1}\right) / \left(e_{C2} - e_{D2}\right) \tag{A4}$$

$$\kappa = \left(e_{D1} e_{C2} - e_{D2} e_{C1}\right) / \left(e_{C2} - e_{D2}\right) \tag{A5}$$

M and κ can be determined from calibrations, and then total dye concentration can be calculated as

$$S_T = \left(F_1 + MF_2\right) / \kappa. \tag{A6}$$

The equations above are simpler than the corresponding equations for the SEER method (Launikonis et al., 2005) because only one excitation light is used with FRET monitors.

M is, essentially, a ratio of quantum yields. By Eq. A4, M is the ratio of loss of fluorescence in the donor range over gain of fluorescence in the acceptor range upon Ca binding. Because in the present configuration, there is little "cross talk" (little donor fluorescence in the acceptor range and vice-versa), the right hand side of Eq. A4 is approximately equal to the ratio caused by FRET of loss of donor fluorescence in the donor range to acceptor fluorescence in the acceptor range. This ratio is given in Gordon et al. (1998), where it is represented by G, as:

$$G = \left(\Phi_A Q_A\right) / \left(\Phi_D Q_D\right), \tag{A7}$$

where Qs are quantum yields of donor (D) or acceptor (A), and Φs are fractions of the donor or acceptor fluorescence transmitted in the corresponding measurement ranges.

One last difficulty in the present case is that all es in the above expressions are fluorescence intensities normalized by sensor concentration. For calibration purposes, we first obtained M by applying Eq. A6 at two times (t_1 and t_2) in line-scan images of cells undergoing large depleting Ca release (for example, Fig. 3). Because S_T is constant:

$$F_1(t_1) + M F_2(t_1) = F_1(t_2) + M F_2(t_2) \quad \text{and}$$

$$M = \left[F_1(t_2) - F_1(t_1)\right] / \left[F_2(t_1) - F_2(t_2)\right]. \tag{A8}$$

With M known, κ was derived by applying Eq. A6 to a solution of known concentration of an equal mixture of ECFP and EYFP, obtained commercially. A similar value for κ was obtained using Eq. A6 with a solution of purified biosensor, concentration derived from donor or acceptor absorbance measurements (which were mutually consistent, as discussed in Materials and methods).

Eq. A6 was used to compute pixel-by-pixel $D_T(x,y)$ images like those shown in Fig. 2 E. Such images could then be used to establish regions with different expression densities, as described with Fig. 8, and calculate corresponding averages of R and $[Ca^{2+}]_{SR}$.

We are grateful to R.Y. Tsien and A.E. Palmer for the gift of D4cpv, to D.-H. Kim for Casq-1 and Casq1-δAsp, and to D. Terentyev and S. Gyorke for pEYFP-N1-dogCasq2. We thank P. D. Allen and S. Pouvreau for criticism of the manuscript and C. Franzini-Armstrong for advice in interpreting images of D1ER expression. We are especially grateful to C. Manno for help at several stages of preparation of the manuscript.

This work was supported by grants from the National Institute of Arthritis and Musculoskeletal and Skin Diseases (AR049184 and AR032808 to E. Ríos, and AR057404 to J. Zhou) and the Muscular Dystrophy Association of America (MDA-4351 to J. Zhou).

Richard L. Moss served as editor.

Submitted: 22 December 2010
Accepted: 28 June 2011

REFERENCES

Afshar, N., B.E. Black, and B.M. Paschal. 2005. Retrotranslocation of the chaperone calreticulin from the endoplasmic reticulum lumen to the cytosol. *Mol. Cell. Biol.* 25:8844–8853. doi:10.1128/MCB.25.20.8844-8853.2005

Agard, D.A., Y. Hiraoka, P. Shaw, and J.W. Sedat. 1989. Fluorescence microscopy in three dimensions. *Methods Cell Biol.* 30:353–377. doi:10.1016/S0091-679X(08)60986-3

Bannwarth, M., I.R. Correa, M. Sztretye, S. Pouvreau, C. Fellay, A. Aebischer, L. Royer, E. Rois, and K. Johnsson. 2009. Indo-1 derivatives for local calcium sensing. *ACS Chem. Biol.* 4:179–190. doi:10.1021/cb800258g

Baylor, S.M., and S. Hollingworth. 2003. Sarcoplasmic reticulum calcium release compared in slow-twitch and fast-twitch fibres of mouse muscle. *J. Physiol.* 551:125–138. doi:10.1113/jphysiol.2003.041608

Bickel, P.J., and K.A. Doksum. 1977. Mathematical Statistics: basic ideas and selected topics. Holden-Day, Inc., Oakland, CA.

Calderón, J.C., P. Bolaños, S.H. Torres, G. Rodríguez-Arroyo, and C. Caputo. 2009. Different fibre populations distinguished by their calcium transient characteristics in enzymatically dissociated murine flexor digitorum brevis and soleus muscles. *J. Muscle Res. Cell Motil.* 30:125–137. doi:10.1007/s10974-009-9181-1

Canato, M., M. Scorzeto, M. Giacomello, F. Protasi, C. Reggiani, and G.J. Stienen. 2010. Massive alterations of sarcoplasmic reticulum free calcium in skeletal muscle fibers lacking calsequestrin revealed by a genetically encoded probe. *Proc. Natl. Acad. Sci. USA.* 107:22326–22331. doi:10.1073/pnas.1009168108

Chen, W., C. Steenbergen, L.A. Levy, J. Vance, R.E. London, and E. Murphy. 1996. Measurement of free Ca2+ in sarcoplasmic reticulum in perfused rabbit heart loaded with 1,2-bis(2-amino-5,6-difluorophenoxy)ethane-N,N,N',N'-tetraacetic acid by 19F NMR. *J. Biol. Chem.* 271:7398–7403. doi:10.1074/jbc.271.13.7398

Dedhar, S. 1994. Novel functions for calreticulin: interaction with integrins and modulation of gene expression? *Trends Biochem. Sci.* 19:269–271. doi:10.1016/0968-0004(94)90001-9

Dedhar, S., P.S. Rennie, M. Shago, C.Y. Hagesteijn, H. Yang, J. Filmus, R.G. Hawley, N. Bruchovsky, H. Cheng, R.J. Matusik, et al. 1994. Inhibition of nuclear hormone receptor activity by calreticulin. *Nature.* 367:480–483. doi:10.1038/367480a0

Demaurex, N., and M. Frieden. 2003. Measurements of the free luminal ER Ca(2+) concentration with targeted "cameleon" fluorescent proteins. *Cell Calcium.* 34:109–119. doi:10.1016/S0143-4160(03)00081-2

DiFranco, M., P. Neco, J. Capote, P. Meera, and J.L. Vergara. 2006. Quantitative evaluation of mammalian skeletal muscle as a heterologous protein expression system. *Protein Expr. Purif.* 47:281–288. doi:10.1016/j.pep.2005.10.018

Fryer, M.W., and D.G. Stephenson. 1996. Total and sarcoplasmic reticulum calcium contents of skinned fibres from rat skeletal muscle. *J. Physiol.* 493:357–370.

Golovina, V.A., and M.P. Blaustein. 1997. Spatially and functionally distinct Ca2+ stores in sarcoplasmic and endoplasmic reticulum. *Science.* 275:1643–1648. doi:10.1126/science.275.5306.1643

Gonzalez, E., M.L. Messi, Z. Zheng, and O. Delbono. 2003. Insulin-like growth factor-1 prevents age-related decrease in specific force and intracellular Ca2+ in single intact muscle fibres from transgenic mice. *J. Physiol.* 552:833–844. doi:10.1113/jphysiol.2003.048165

Gordon, G.W., G. Berry, X.H. Liang, B. Levine, and B. Herman. 1998. Quantitative fluorescence resonance energy transfer measurements using fluorescence microscopy. *Biophys. J.* 74:2702–2713. doi:10.1016/S0006-3495(98)77976-7

Holaska, J.M., B.E. Black, D.C. Love, J.A. Hanover, J. Leszyk, and B.M. Paschal. 2001. Calreticulin Is a receptor for nuclear export. *J. Cell Biol.* 152:127–140. doi:10.1083/jcb.152.1.127

Inesi, G. 1994. Teaching active transport at the turn of the twenty-first century: recent discoveries and conceptual changes. *Biophys. J.* 66:554–560. doi:10.1016/S0006-3495(94)80872-0

Jiménez-Moreno, R., Z.M. Wang, M.L. Messi, and O. Delbono. 2010. Sarcoplasmic reticulum Ca^{2+} depletion in adult skeletal muscle fibres measured with the biosensor D1ER. *Pflugers Arch.* 459:725–735. doi:10.1007/s00424-009-0778-4

Jong, D.S., P.C. Pape, W.K. Chandler, and S.M. Baylor. 1993. Reduction of calcium inactivation of sarcoplasmic reticulum calcium release by fura-2 in voltage-clamped cut twitch fibers from frog muscle. *J. Gen. Physiol.* 102:333–370. doi:10.1085/jgp.102.2.333

Kabbara, A.A., and D.G. Allen. 2001. The use of the indicator fluo-5N to measure sarcoplasmic reticulum calcium in single muscle fibres of the cane toad. *J. Physiol.* 534:87–97. doi:10.1111/j.1469-7793.2001.00087.x

Kettlun, C., A. González, E. Ríos, and M. Fill. 2003. Unitary Ca2+ current through mammalian cardiac and amphibian skeletal muscle ryanodine receptor Channels under near-physiological ionic conditions. *J. Gen. Physiol.* 122:407–417. doi:10.1085/jgp.200308843

Launikonis, B.S., J. Zhou, L. Royer, T.R. Shannon, G. Brum, and E. Ríos. 2005. Confocal imaging of [Ca2+] in cellular organelles by SEER, shifted excitation and emission ratioing of fluorescence. *J. Physiol.* 567:523–543. doi:10.1113/jphysiol.2005.087973

Launikonis, B.S., J. Zhou, L. Royer, T.R. Shannon, G. Brum, and E. Ríos. 2006. Depletion "skraps" and dynamic buffering inside the cellular calcium store. *Proc. Natl. Acad. Sci. USA.* 103:2982–2987. doi:10.1073/pnas.0511252103

Mejía-Alvarez, R., C. Kettlun, E. Ríos, M. Stern, and M. Fill. 1999. Unitary Ca2+ current through cardiac ryanodine receptor channels under quasi-physiological ionic conditions. *J. Gen. Physiol.* 113:177–186. doi:10.1085/jgp.113.2.177

Messerli, J.M., H.T. van der Voort, E. Rungger-Brändle, and J.C. Perriard. 1993. Three-dimensional visualization of multi-channel volume data: the amSFP algorithm. *Cytometry.* 14:725–735. doi:10.1002/cyto.990140705

Miyawaki, A., J. Llopis, R. Heim, J.M. McCaffery, J.A. Adams, M. Ikura, and R.Y. Tsien. 1997. Fluorescent indicators for Ca2+ based on green fluorescent proteins and calmodulin. *Nature.* 388:882–887. doi:10.1038/42264

Murphy, R.M., N.T. Larkins, J.P. Mollica, N.A. Beard, and G.D. Lamb. 2009. Calsequestrin content and SERCA determine normal and maximal Ca2+ storage levels in sarcoplasmic reticulum of fast- and slow-twitch fibres of rat. *J. Physiol.* 587:443–460. doi:10.1113/jphysiol.2008.163162

Owen, V.J., G.D. Lamb, D.G. Stephenson, and M.W. Fryer. 1997. Relationship between depolarization-induced force responses and Ca2+ content in skeletal muscle fibres of rat and toad. *J. Physiol.* 498:571–586.

Palmer, A.E., and R.Y. Tsien. 2006. Measuring calcium signaling using genetically targetable fluorescent indicators. *Nat. Protoc.* 1:1057–1065. doi:10.1038/nprot.2006.172

Palmer, A.E., M. Giacomello, T. Kortemme, S.A. Hires, V. Lev-Ram, D. Baker, and R.Y. Tsien. 2006. Ca2+ indicators based on computationally redesigned calmodulin-peptide pairs. *Chem. Biol.* 13:521–530. doi:10.1016/j.chembiol.2006.03.007

Pape, P.C., D.S. Jong, W.K. Chandler, and S.M. Baylor. 1993. Effect of fura-2 on action potential-stimulated calcium release in cut twitch fibers from frog muscle. *J. Gen. Physiol.* 102:295–332. doi:10.1085/jgp.102.2.295

Pape, P.C., K. Fénelon, C.R. Lamboley, and D. Stachura. 2007. Role of calsequestrin evaluated from changes in free and total calcium concentrations in the sarcoplasmic reticulum of frog cut skeletal muscle fibres. *J. Physiol.* 581:319–367. doi:10.1113/jphysiol.2006.126474

Pickart, C.M., and W.P. Jencks. 1984. Energetics of the calcium-transporting ATPase. *J. Biol. Chem.* 259:1629–1643.

Pizarro, G., and E. Ríos. 2004. How source content determines intracellular Ca2+ release kinetics. Simultaneous measurement of [Ca2+] transients and [H+] displacement in skeletal muscle. *J. Gen. Physiol.* 124:239–258. doi:10.1085/jgp.200409071

Ríos, E., B.S. Launikonis, L. Royer, G. Brum, and J. Zhou. 2006. The elusive role of store depletion in the control of intracellular calcium release. *J. Muscle Res. Cell Motil.* 27:337–350. doi:10.1007/s10974-006-9082-5

Rojiani, M.V., B.B. Finlay, V. Gray, and S. Dedhar. 1991. In vitro interaction of a polypeptide homologous to human Ro/SS-A antigen (calreticulin) with a highly conserved amino acid sequence in the cytoplasmic domain of integrin alpha subunits. *Biochemistry.* 30:9859–9866. doi:10.1021/bi00105a008

Royer, L., S. Pouvreau, and E. Ríos. 2008. Evolution and modulation of intracellular calcium release during long-lasting, depleting depolarization in mouse muscle. *J. Physiol.* 586:4609–4629. doi:10.1113/jphysiol.2008.157990

Royer, L., M. Sztretye, C. Manno, S. Pouvreau, J. Zhou, B.C. Knollmann, F. Protasi, P.D. Allen, and E. Ríos. 2010. Paradoxical buffering of calcium by calsequestrin demonstrated for the calcium store of skeletal muscle. *J. Gen. Physiol.* 136:325–338. doi:10.1085/jgp.201010454

Rudolf, R., P.J. Magalhães, and T. Pozzan. 2006. Direct in vivo monitoring of sarcoplasmic reticulum Ca^{2+} and cytosolic cAMP dynamics in mouse skeletal muscle. *J. Cell Biol.* 173:187–193. doi:10.1083/jcb.200601160

Schneider, M.F., B.J. Simon, and G. Szucs. 1987. Depletion of calcium from the sarcoplasmic reticulum during calcium release in frog skeletal muscle. *J. Physiol.* 392:167–192.

Shin, D.W., J. Ma, and D.H. Kim. 2000. The asp-rich region at the carboxyl-terminus of calsequestrin binds to $Ca^{(2+)}$ and interacts with triadin. *FEBS Lett.* 486:178–182. doi:10.1016/S0014-5793(00)02246-8

Sztretye, M., J. Yi, L. Figueroa, J. Zhou, L. Royer, P.D. Allen, and E. Ríos. 2011. Permeability of the calcium store membrane and its changes during function, directly measured in mouse skeletal muscle cells. *J. Gen. Physiol.* 138:231–247.

Terentyev, D., S. Viatchenko-Karpinski, I. Györke, P. Volpe, S.C. Williams, and S. Györke. 2003. Calsequestrin determines the functional size and stability of cardiac intracellular calcium stores: Mechanism for hereditary arrhythmia. *Proc. Natl. Acad. Sci. USA.* 100:11759–11764. doi:10.1073/pnas.1932318100

van der Voort, H.T.M., and K.C. Strasters. 1995. Restoration of confocal images for quantitative image-analysis. *Journal of Microscopy (Oxford).* 178:165–181.

Wang, Z.M., M.L. Messi, and O. Delbono. 1999. Patch-clamp recording of charge movement, Ca2+ current, and Ca2+ transients in adult skeletal muscle fibers. *Biophys. J.* 77:2709–2716. doi:10.1016/S0006-3495(99)77104-3

Wu, Y.C., T. Tucker, and R. Fettiplace. 1996. A theoretical study of calcium microdomains in turtle hair cells. *Biophys. J.* 71:2256–2275. doi:10.1016/S0006-3495(96)79429-8

Zima, A.V., E. Bovo, D.M. Bers, and L.A. Blatter. 2010. Ca^{2}+ spark-dependent and -independent sarcoplasmic reticulum Ca^{2}+ leak in normal and failing rabbit ventricular myocytes. *J. Physiol.* 588:4743–4757. doi:10.1113/jphysiol.2010.197913

Ziman, A.P., C.W. Ward, G.G. Rodney, W.J. Lederer, and R.J. Bloch. 2010. Quantitative measurement of Ca^{2}(+) in the sarcoplasmic reticulum lumen of mammalian skeletal muscle. *Biophys. J.* 99:2705–2714. doi:10.1016/j.bpj.2010.08.032

Published July 25, 2011

Sztretye et al., http://www.jgp.org/cgi/content/full/jgp.201010591/DC1

Example cell with low density of biosensor

Fig. S1 illustrates a stack of images of an additional cell, with the same optical and acquisition parameters used for the dual-stain experiment in Fig. 1. The lower level and heterogeneity of expression of D4cpv-δAsp in this cell results in a clear view of the di-8-ANEPPS staining in the interior of the cell. The figure also shows, in panels A and B, a pair of raw images, near the center of the z stacks used in the 3D reconstruction. The plots in F confirm the colocalization of biosensor and t tubule stain. The first 4 µm of the profiles in F are plotted in G, rescaled, and vertically shifted to match both maxima and minima. Horizontal line a is traced at the average maximum and line b at one-half of that value. Half widths of the bands of both signals are measured on line b. Their averages for the three full bands shown are 0.400 µm for the biosensor (SEM = 0.0058) and 0.326 (SEM = 0.0067) for di-8-ANEPPS. The difference, 0.074 µm, is highly significantly different from 0, a result consistent with a location of the biosensor in the terminal cisternae of the SR.

Structural aspects of the expression of D1ER

Figs. S2–S5 illustrate features of D1ER, as seen in mice 4–7 d after transfection. Approximately 50% of the cells showed fluorescence with the emission spectrum of D1ER. In every case, the extrinsic fluorescence appeared throughout the length and width of the fiber, showing the structural pattern illustrated in Fig. S2 A. This "pattern I" is shown in a 3-D rendering (analogous to that used for Fig. 1) in Fig. 2 D. Pattern I was identified in all cells expressing D1ER examined at high magnification (46, from 6 transfected mice).

The cell illustrated in Fig. S2 A was costained with Mitrotracker Deep Red. The simultaneously acquired image of this stain is shown in Fig. S2 B, showing the characteristic double row of mitochondria. In mammalian skeletal muscle, mitochondria are mostly transversal to the fiber and form a band that largely overlaps with but is narrower than the "I-Z-I" section of the SR. The center of the mitochondrial band therefore locates the z line. The overlay (Fig. S2 C) demonstrates that the transversal band of high D1ER expression colocates with the z line.

Nearly 30% of the cells expressing D1ER also presented areas with fluorescence of identical emission spectrum in a different spatial pattern, "pattern II." The typical appearance of this pattern is illustrated with Figs. S3 and S4. The presentation of pattern II was always in segments or patches, usually <200 µm long, which often did not span the diameter of the fiber. As illustrated with the wide-field transmitted light image of Fig. S3 A, the region of the cell expressing pattern II was usually not deformed or altered perceptibly. As illustrated by the wide-field fluorescence image in Fig. S3 B, the intensity of fluorescence in these regions was much greater than in the rest of the cell (typically 10 times greater). The other areas of the fibers expressing pattern II always expressed D1ER fluorescence, and always with pattern I. This is illustrated with Fig. S3 C, in which fluorescence of the same cell, acquired with greater gain, is displayed using a color palette designed to visualize the areas of low fluorescence. A portion of those areas (in a box in Fig. S3 C) is displayed magnified in Fig. S3 D, and shows the characteristic transversal striation of pattern I.

The large difference of intensity between areas with different patterns of expression raised the concern that intrinsic (auto) fluorescence might be confusing the results. Specific measurements were done in unstained, untransfected cells, and showed that the levels of autofluorescence were at least 20 times lower than those typical for pattern I (probably because light of 458 nm is a poor exciter of autofluorescence). In addition, autofluorescence had different emission spectrum and structural pattern.

To clarify the locations in the sarcomere of the areas of high D1ER density, cells with dual pattern were costained with di-8-ANEPPS. An individual low-resolution image of the biosensor is shown in Fig. S4 A, and the simultaneously obtained image of di-8-ANEPPS is shown in B. Fig. S4 A shows the coexistence of the two patterns (pattern I is present in the lower-right corner) and illustrates the transition between the two, which was always sharp, usually occupying no more, and often much less, than 5 µm in every direction. Fig. S4 (C and D) shows 3-D renderings of z stacks of D1ER and di-8-ANEPPS fluorescence acquired simultaneously. The stacks cover a region of pattern I expression (bottom half of images) and one of pattern II (top). They also show clearly the sharp transition between patterns. The joint 3-D display (Fig. S4 E) shows that in the area of pattern I there is little overlap between biosensor and tubules. The overlap is greater where D1ER adopts pattern II. The plots in Fig. S4 F are "profiles" of expression in the x (longitudinal) direction, calculated within the box in Fig. 4 E. The profiles show substantial overlap of biosensor and t tubules, but they also reveal a subtle shift, systematically repeated in every sarcomere. Because of the shift, the t tubules, while partly covered, are still visible in the joint 3-D rendering of Fig. S4 E (compare with Fig. 1 E, where they are entirely covered by D4cpv).

In several cells, the sharp border between areas of different expression pattern featured a "Vernier shift" of the stack of t tubules. Such a shift is clear in the right half of Fig. S4 D, but is not present in the left half of the image, which suggests that discontinuity of the t tubule array is not the cause of the pattern transition.

FRET responses of D1ER in muscle cells

Initial tests consisted in the application of the release cocktail to quiescent cells. Fig. S5 illustrates an example. Fig. S5 (A and B) displays the images F_1 (donor) and F_2 (acceptor). Fig. S5 C plots the "invariant" combination of F_1 and F_2, which is proportional to the concentration of biosensor, as described in Materials and methods and the Appendix. Fig. S5 D is their ratio $R(x,y)$, which has an average value of 1.99. The cell was then exposed to the release cocktail (described in Materials and methods) and imaged after 5 min. The four lower panels document the changes. The biosensor concentration image evidenced some movement but little change otherwise. The $R(x,y)$ image, in Fig. S5 F, had an average value of 1.37. This change is representative of results in four cells (average at rest, 1.79; SEM, 0.10; average after release, 1.39; SEM, 0.02). The largest value of R found in 12 cells at rest was 2.50 (average, 1.93; SEM, 0.11). Assuming R_{min} = 1.39, R_{max} = 2.50, $DR((R_{max}\text{-}R_{min})/R_{min})$ = 0.80.

Published July 25, 2011

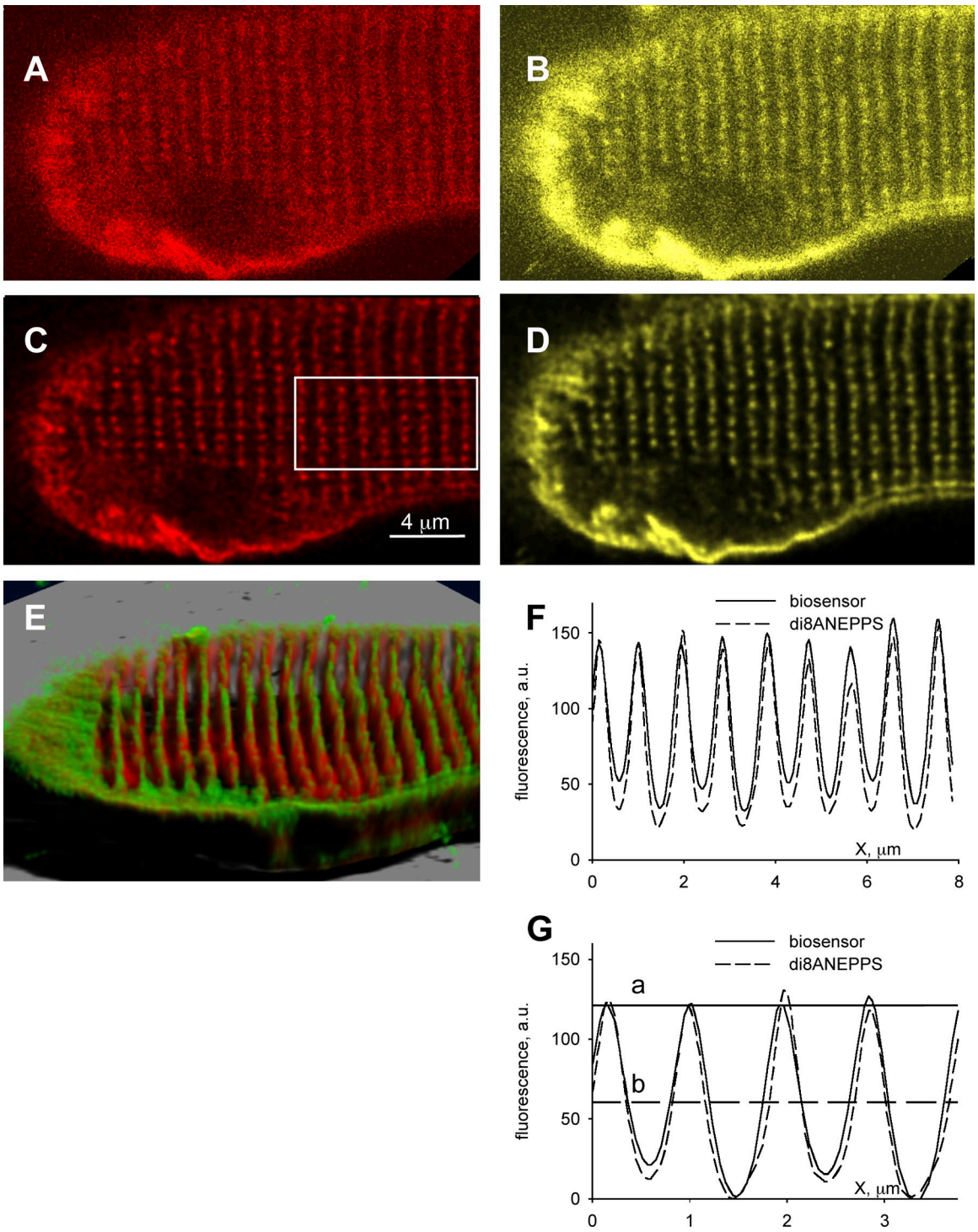

Figure S1. 3D reconstructions in a cell expressing a D4cpv fusion at low concentration. The figure illustrates two z stacks of 30 images each of a cell expressing D4cpv-δAsp, costained with di-8-ANEPPS. Successive images were obtained simultaneously for the two stacks. (A and B) Individual unprocessed images at position 13. (A) Biosensor. (B) di-8-ANEPPS. (C and D) Corresponding images after deblurring. (E) 3-D rendering by the SFP algorithm. Note that t tubules are visible, especially near the fiber axis, where biosensor concentration is lowest. (F) Fluorescence in C and D averaged over coordinate y in the boxed area. Note that the profiles of di-8-ANEPPS are visibly narrower than those of the colocalized biosensor. ID: 020411a series 138, slice 13.

Published July 25, 2011

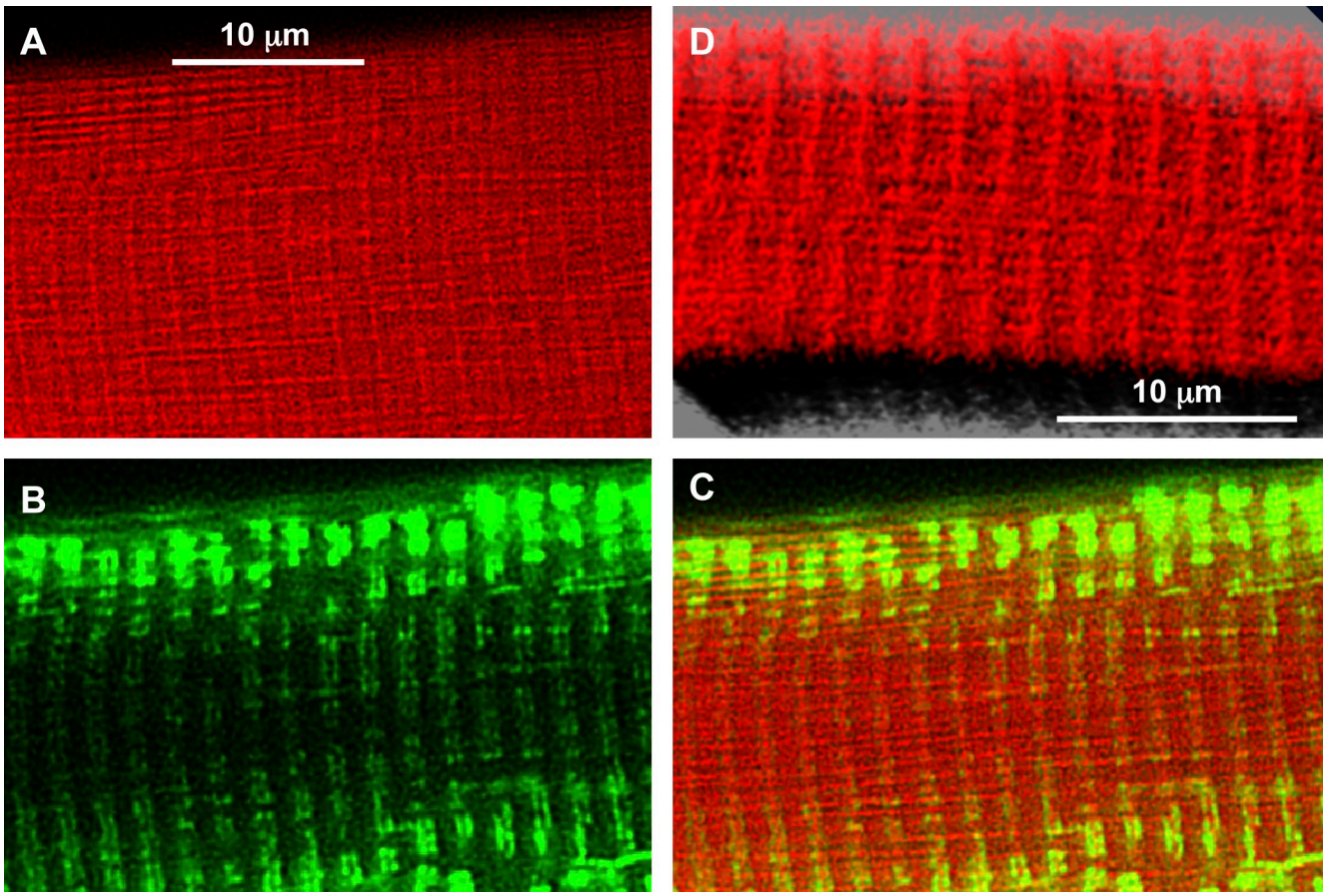

Figure S2. The dominant pattern of expression of D1ER. (A) Single image of fluorescence in a cell expressing D1ER. Wavelengths of excitation and emission were the same as those used for D4cpv. (B) Simultaneously obtained image of Mitotracker Deep Red (Ex, 633 nm; Em, 650–750 nm). Note the double rows of mitochondria, which in mammalian muscle are near the center of the I band. (C) Overlay of images of A and B. Note the colocalization of the transversal band of high biosensor expression with mitochondria, which locates the biosensor band near the z line. ID: 042106a series 102. (D) 3-D rendering of a stack of images of D1ER fluorescence in a different cell, revealing the placement of the biosensor in irregular sacs arranged longitudinally, and a transversal band of high expression density, which is centered at the z line (as shown with C). ID: 020911c series 13.

Published July 25, 2011

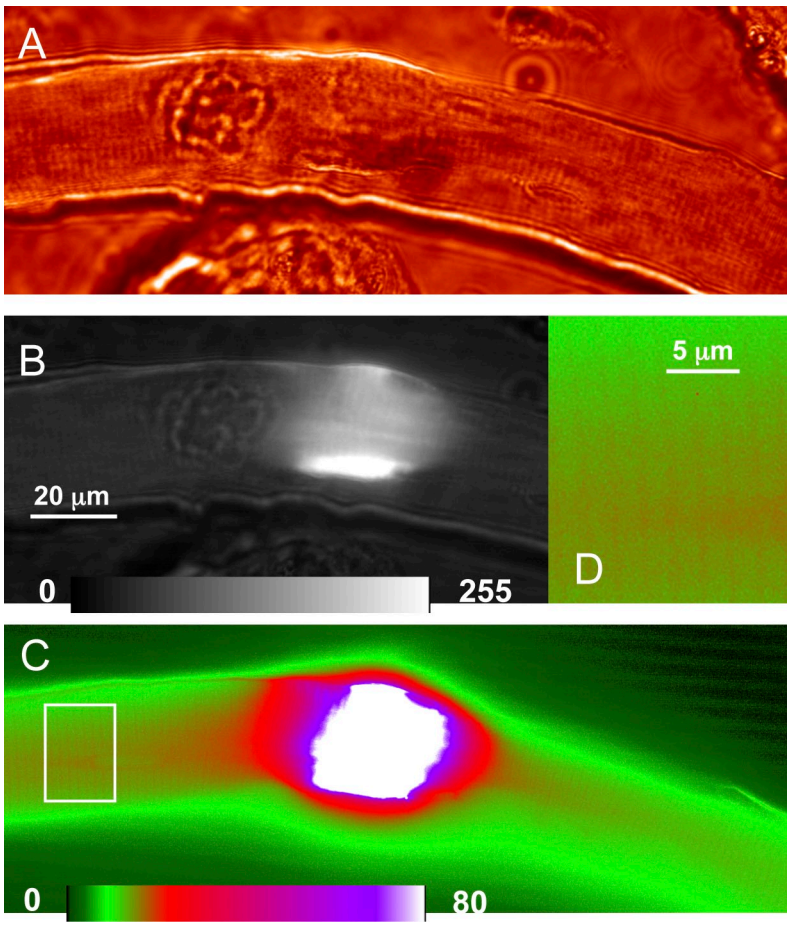

Figure S3. D1ER expressed in two patterns; wide-field images. (A) Transmitted light wide-field image. (B) Fluorescence wide-field image. Both images were displayed unprocessed. (C) Wide-field image of fluorescence, displayed with amplified intensity, in a color scale chosen for optimal resolution of low-intensity fluorescence. (D) Magnified view of the boxed region in C, showing fluorescence with D1ER pattern I. The central area of high expression was found to have pattern II in images obtained with lower excitation intensity. ID: 021611f, camera 0, 2, 12.

Published July 25, 2011

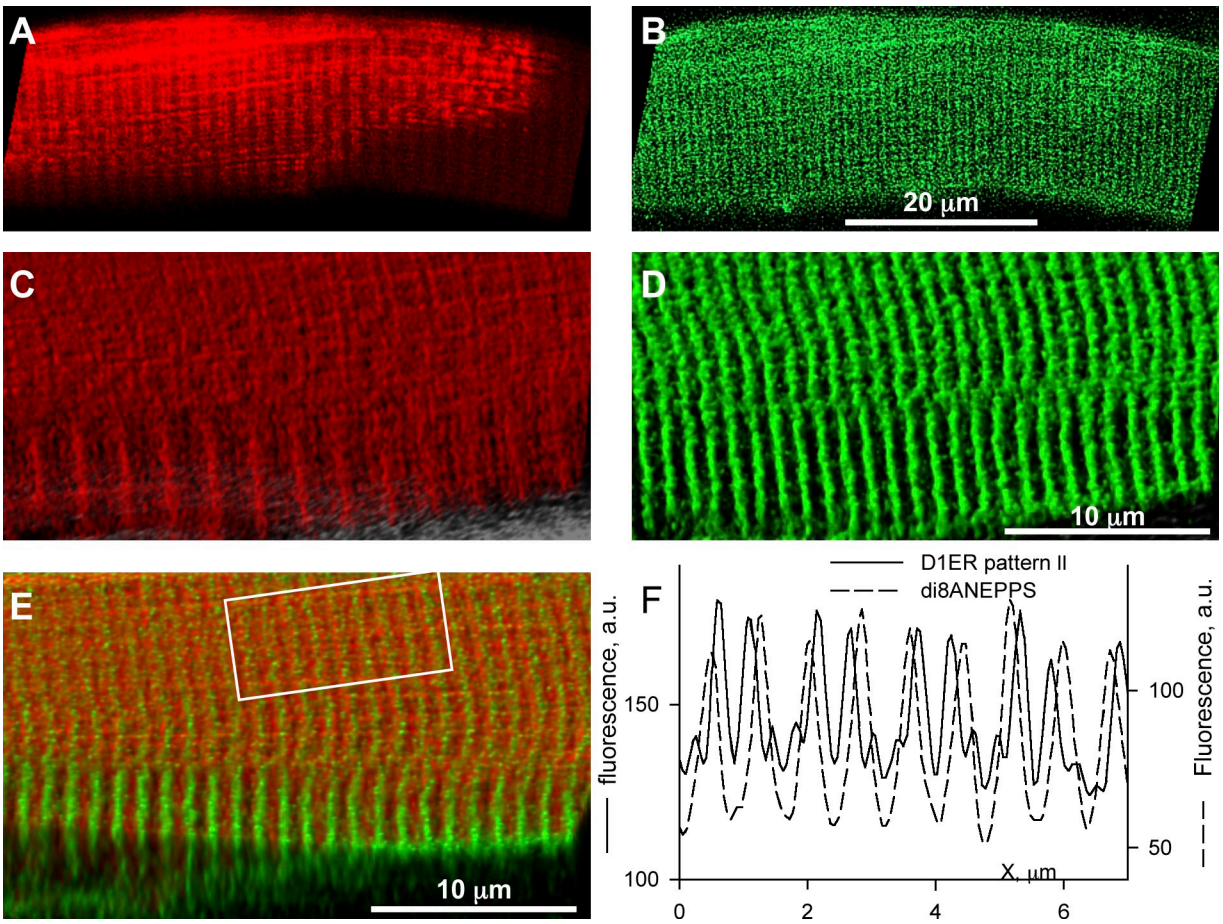

Figure S4. D1ER expressed in two different patterns; confocal images. (A) Biosensor fluorescence. (B) di-8-ANEPPS fluorescence in a cell expressing D1ER, costained as described in the legend for Fig. S1. The images were obtained simultaneously at low magnification. Pattern I is present at the bottom and lower right. Pattern II is spatially different and of much greater intensity. (C and D) 3-D renderings of z stacks obtained in the same cell, at higher magnification. Processing was as described for Fig. 2 and Fig. S1, with the same display parameters. Note in C the sharp transition between patterns I, at the bottom, and II at the top of the panel. Note that part of the border between the areas of different patterns coincides with a "Vernier shift" in alignment of t tubules. This shift, however, is not present in the left half of the image, where the transition is sharpest. (E) Joint 3-D rendering of both stacks. Note that D1ER in pattern II colocalizes better with t tubules, but still colocalizes imperfectly. (F) Profiles of fluorescence, averaged transversally within the area marked by the box in E. Note the slight but systematic shift between peaks of biosensor expression and t tubules. ID: A and B, 020911d images 18; C–F, 020911d series 35.

Published July 25, 2011

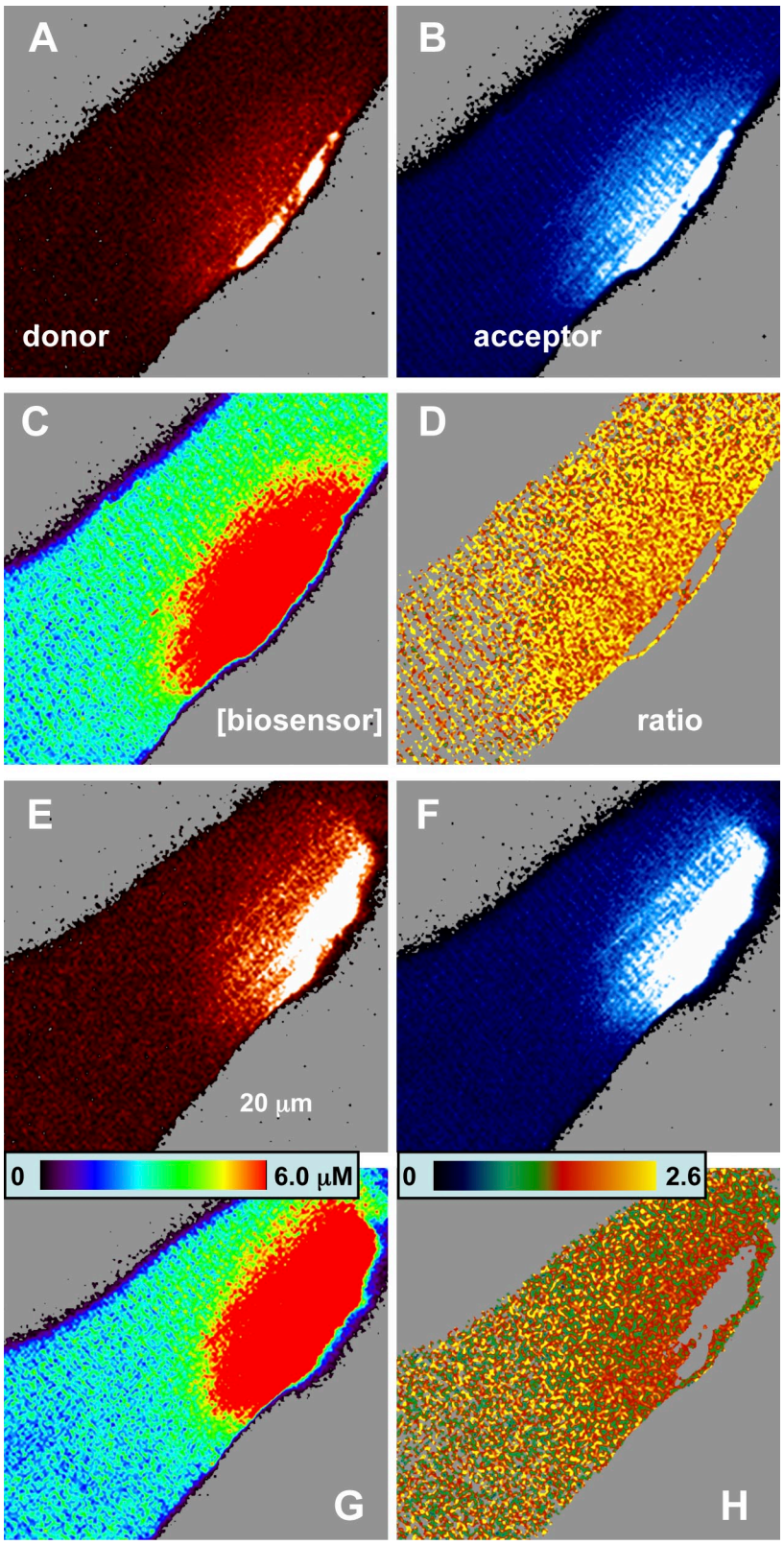

Figure S5. Response of D1ER. (A and B) FRET pair of fluorescence images of a fiber expressing D1ER. (C) The ratio *R* of B over A, after background subtraction. (D) Image of biosensor concentration (scale is based on calibration described in the Appendix). (E) Image of biosensor concentration after application of the "release cocktail" (Materials and methods). (F) *R* after cocktail; calculation was restricted to areas where [biosensor] was greater than the mean minus 1 standard deviation of the distribution of [biosensor]. The average *R* went from 1.99 in C to 1.37 in F. ID: 021811b, images 14 and 22.